Journal Pre-proof

Wearable Fiber-Based Thermoelectrics from Materials to Applications

Wen-Yi Chen, Xiao-Lei Shi, Jin Zou, Zhi-Gang Chen

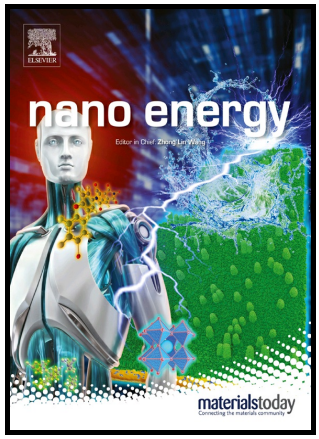

PII: S2211-2855(20)31257-X

DOI: https://doi.org/10.1016/j.nanoen.2020.105684

Reference: NANOEN105684

To appear in: *Nano Energy*

Received date: 14 October 2020
Revised date: 1 December 2020
Accepted date: 9 December 2020

Please cite this article as: Wen-Yi Chen, Xiao-Lei Shi, Jin Zou and Zhi-Gang Chen, Wearable Fiber-Based Thermoelectrics from Materials to Applications, *Nano Energy,* (2020) doi:https://doi.org/10.1016/j.nanoen.2020.105684

Wearable Fiber-Based Thermoelectrics from Materials to Applications

Wen-Yi Chen,[a,#] Xiao-Lei Shi,[b,#] Jin Zou,[a,c] and Zhi-Gang Chen[b,a*]*

[a] School of Mechanical and Mining Engineering, The University of Queensland, St Lucia, QLD 4072, Australia

[b] Centre for Future Materials, University of Southern Queensland, Springfield Central, QLD 4300, Australia.

[c] Center for Microscopy and Microanalysis, The University of Queensland, St Lucia, QLD 4072, Australia

[#] These authors contribute equally for this work.

Corresponding Author

* zhigang.chen@usq.edu.au (ZGC) and j.zou@uq.edu.au (JZ).

Abstract

Thermoelectrics, enabling direct converting between heat and electricity, have become one of the most promising techniques for the realization of energy-saving and environmental protection. As a key member of the thermoelectric family, fiber-based thermoelectrics possess significant potential in the area of charging wearable electronics, owing to their high performance, high flexibility, and high stability features. Based on the fast development of fiber-based thermoelectrics, this review aims to comprehensively summarize the state-of-the-art fiber-based thermoelectric materials and devices, including their unique designs, chemical engineering, advanced fabrication methods, outstanding

thermoelectric properties, and wide applications. In the end, we point out the challenge and outlook for further improving thermoelectric performance, flexibility, and stability of fiber-based thermoelectrics.

Keywords: thermoelectric; fiber; performance; design; fabrication.

Table of Content

Introduction

Owing to the rapid development of smart wearable electronics such as smartwatches and internal pacemakers, demands for flexible and wearable energy sources are explosively rising [1]. Most of these technologies are focusing on weight-light and high-flexibility, and also promise self-powering by effectively converting human-body energy into electricity. **Figure 1(a)** illustrates the powers produced by the human body [2]. According to the statistics [2], the human body can generate >100 W power energy for a 68 Kg adult. Fortunately, only 1 % conversion efficiency from human body energy can satisfy most of the implant or portable electronics, such as cochlear implants, heart pacemakers, gastric simulators, smart glasses, activity trackers, and smartwatch, as illustrated in **Figure 1(b)**) [3]. Therefore, searching for cost-effective energy conversion technology has become a key research direction for wearable electronics.

The development of thermoelectric materials and devices has risen rapidly, because of their unique characteristics including solid-state conversion, silence, and no moving parts [4-6]. Most traditional thermoelectric materials are in the form of rigid devices [1, 7]. Increasing interests are to reduce the size of thermoelectric devices and also increase their entire thermoelectric conversion efficiency. However, the current low thermoelectric conversion efficiency has restricted their wider applications. Other shortcomings for developed inorganic thermoelectric materials are their high cost and toxic nature [8]. With the rapid development of technology and the increasing demand for wearable electronics, more attentions have been moved towards the self-power and maintenance-free systems. Flexible

thermoelectric generators (F-TEGs) can tightly adhere to human skins, and may generate maintenance-free electricity based on the direct conversion of the temperature difference between the human body and ambient temperature.

Generally, inorganic thermoelectric materials, such as PbTe [9-16], Cu_2Se [17-27], GeTe [28-39], SnSe [40-54], SnTe [11, 35, 55-63], and Bi_2Te_3 [64-75], have higher figure-of-merit (*ZT*) than that of organic thermoelectric materials [76], but their rigid and brittle properties symbolize that inorganic thermoelectric materials need substrates to make them flexibility. In contrast, organic thermoelectric materials have unique properties containing excellent flexibility, low thermal conductivity (κ), low cost, and convenient processing, making them as promising thermoelectric candidates [77]. So far, many methods have been developed to combine organic and inorganic materials to ensure high thermoelectric performance and high flexibility [1, 78].

Compared to conventional F-TEGs, fiber-based wearable F-TEGs can be bent through various directions since fiber-based F-TEGs have excellent tensile, ductile, and in-plane shear properties [78], so that it can be easily attached to an arbitrarily shaped surface such as the human body, as shown in **Figure 1(c)** [78]. The fibers can be treated as advanced thermoelectric materials with both high *ZT*s and high flexibility for applying to flexible thermoelectric devices as thermoelectric "legs", as illustrated in **Figure 1(d)** [78]. At the same time, fibers with good wearability can also be used as flexible substrates for supporting thermoelectric devices to improve the wearability, as shown in **Figure 1(e)** [79]. To date, many fiber-based thermoelectric materials have been developed, and their thermoelectric performances are considerably increasing, as summarized in **Figure 1(d)** [80-93]. The current maximum *ZT* of fiber-based thermoelectric materials can reach 2, realized by the SnSe core fiber [84].

Considering that there is still a lack of a timely review on fiber-based thermoelectric materials and devices, in this work, we overview the state-of-the-art fiber-based thermoelectric materials and devices

targeting wearable electronics. We illustrate the details on the material synthesis, characterizations, thermoelectric properties, device assembly, device performance, and potential applications of fiber-based devices. Finally, we point out the challenges and outlook of fiber-based thermoelectrics.

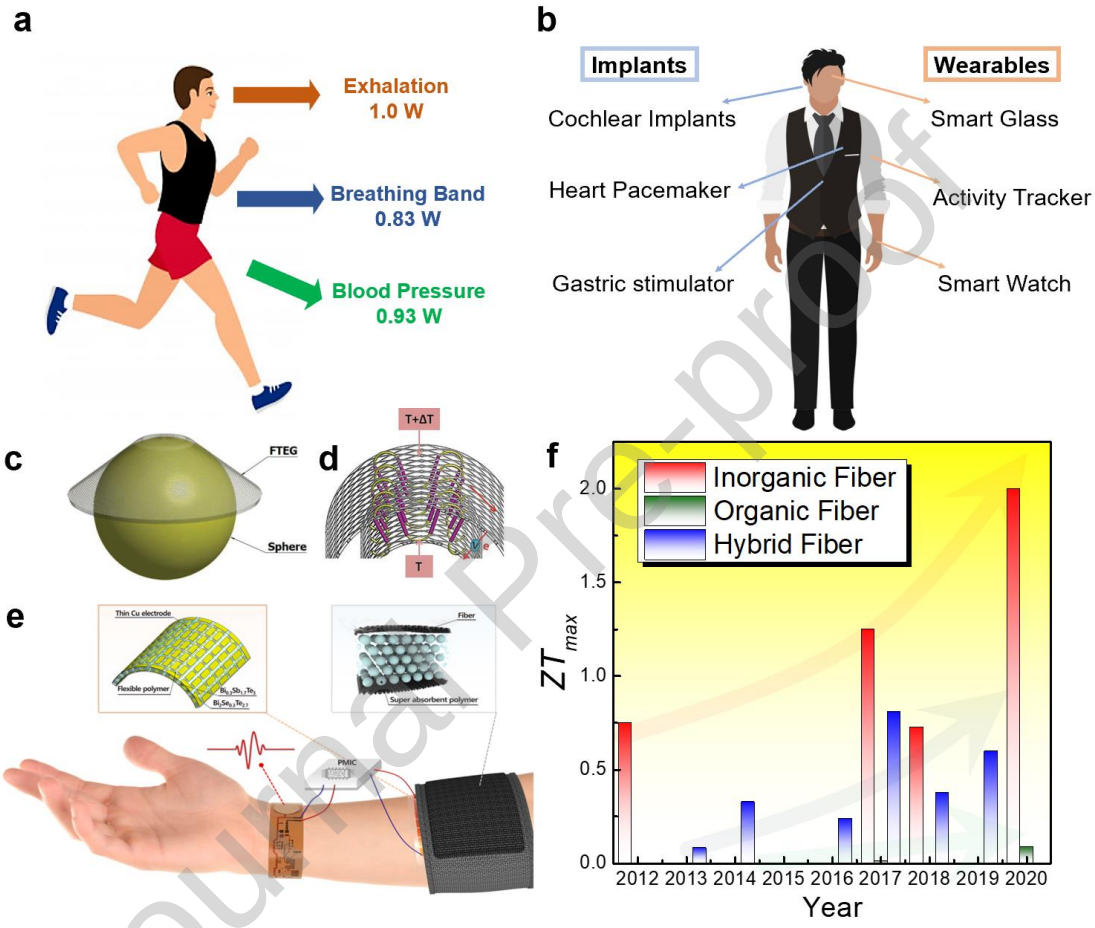

Figure 1. Illustrations of (a) the powers produced by the human body [2] and (b) typical applications of wearable electronics. (c) A typical flexible thermoelectric generator (F-TEG) on a sphere. (d) The unit of the fiber-based F-TEG composed of thermoelectric yarns as thermoelectric legs. Reproduced with permission [78]. Copyright 2018 Wiley-VCH. (e) A wearable thermoelectric power generator with a fiber-based flexible substrate for self-powered electrocardiography. Reproduced with permission [79]. Copyright 2018 American Chemical Society. (f) The reported maximum ZT (ZT_{max}) for the fiber-based thermoelectric materials in recent years [80-93].

Fundamental of Fiber-based Thermoelectrics

Thermoelectric Principles

The fundamental of fiber-based F-TEGs is based on the Seebeck effect [94]. The thermoelectric voltage is generated when there exists a temperature difference (ΔT) between both sides (human body and ambient environment), so that the Seebeck effect can be used to generate electricity, measure temperature or change the temperature of objects. For fiber-based thermoelectric materials, their thermoelectric potentials can be evaluated by the dimensionless figure-of-merit ZT values, defined as [95]:

$$ZT = S^2\sigma T/\kappa \tag{1}$$

where σ is the electrical conductivity, S is the Seebeck coefficient, and T is the absolute temperature. Here, $S^2\sigma$ is the power factor and represents the thermoelectric potential from an electrical aspect [96]. As shown in equation (1), ZT is highly related to S, σ, and κ, in which lattice vibrations and electron motions are closely related to κ, expressed by [4]:

$$\kappa = \kappa_l + \kappa_e \tag{2}$$

where κ_l is the lattice thermal conductivity κ_e, and κ_e expresses the electron thermal conductivity [97]. Moreover, σ expresses the motion of electrons, determined by [98]:

$$\sigma = ne\mu \tag{3}$$

where e is the carrier charge and μ is the carrier mobility, and n is the carrier concentration that represents the number of electrons in the conduction band (CB) or the number of holes in the valence band (VB) in thermoelectric materials. In p-type materials, the major carriers are holes, therefore the carrier concentration can be described as n_p. Oppositely, in n-type materials, the major carriers are electrons, therefore the carrier concentration can be described as n_e. Generally, n is significantly affected

by the bandgap and temperature of materials. Carriers in the large bandgap of materials are hard to be generated by the thermal energy, meaning low n [99]. Because S and σ are strongly coupled with each other, a rationally tuned n value is of significance to achieve a high $S^2\sigma$ and a high ZT, as shown in **Figure 2(a)**.

Because κ_l has a weak dependence on n, it is often needed to suppress the κ_l by rational micro/nanostructural designs. Moreover, phonon scatterings depend on temperatures, and phonon transports can significantly affect thermoelectric performance according to equation (1). Grain boundary phonon scattering is significant in the low temperature and Umklapp scattering becomes dominant in the high temperature, as shown in **Figure 2(b)** [100]. More phonon-boundary scattering and electron-phonon scattering can affect phonon transports, leading to low κ of thermoelectric materials [1]. According to Equations (1), (2), and (3), ideal thermoelectric materials should have high σ with low κ to effectively generate more electrical power at a given temperature difference. Such a characteristic is significantly relevant to fiber-based materials and F-TEGs which are targeting for human body heat at a relatively low temperature difference between the surrounding environment and the human body [101, 102].

Flexibility

In addition to the high thermoelectric performance, flexibility is another important factor to ensure fiber-based F-TEGs to be easily assembled and adhered to human skins closely under the fact that the various stretching and bending are loading due to the human motion. Because some F-TEGs are composed of thermoelectric textiles and yarns and fabricated by weaving and knitting, thermoelectric fibers and yarns are the main focuses in this review. The basic criteria to evaluate the quality of fibers/yarns are their flexibility and strength.

Flexibility defines a bending and stretching level of fibers/yarns [103]. A higher level demonstrates higher flexibility, which means that fibers/yarns can be easier to be deformed [104]. Strength defines a twisting level of fibers/yarns, and the number of turns that can be twisted per unit length is the critical criterion to evaluate the strength of fibers/yarns [104]. **Figure 2(c)** illustrates a typical twisting process of fibers/yarns, in which a single produced fiber/yarn needs to be twisted into fibers and then applies the two rolls to twist the two fibers to test their strength. However, the appropriate strength of fibers/yarns is not easily achieved since the strength is closely related to the diameter of yarns, and different materials with different densities need to match the appropriate diameter and length to obtain the demand strength of fibers. The inappropriate diameter of fibers can result in coarse and stiff fibers that have high resistance to bending and twisting, leading to failure in weaving and knitting. Hence, the appropriate diameter is normally determined according to the different materials with the different linear densities in the yarn engineering and then test the level of strength of the fibers through the twisting process. The diameter of yarns can be expressed and estimated [104]:

$$d = \frac{1}{k\sqrt{\rho N}} \tag{4}$$

where N is the volumetric density of a fiber/yarn, and ρ is the linear density of a fiber/yarn.

In addition to the strength and fiber diameter, the interaction between fibers/yarns and skins is also regarded as an important factor to define flexibility. Interaction between fibers/yarns and skins is mainly defined by friction. Appropriate friction can directly affect comfortability. For example, fabrics made of more coarse and rigid fibers/yarns can bring a painful prickling effect on human skins [104]. Except for directly changing materials, strength, and diameter of fibers, friction can be reduced by adjusting fiber orientation and alignment to result in a smoother surface of fibers. Accordingly, the development of fiber-based F-TEGs must combine both fiber/yarn engineering and thermoelectric principles, so that

challenge of the development of fiber-based F-TEGs is significant, needing not only to improve the flexibility of the thermoelectric fibers but also to ensure that the bending and twisting cannot affect the thermoelectric performance of fibers/yarns.

Wearability

Similar to flexibility, wearability is also a critical factor to define whether the fiber-based F-TEGs can be worn by the human. Wearability is mainly divided by toxicity and durability. Toxicity is important because fiber-based F-TEGs are designed to be worn by human body and even put into the internal human body as medical devices. Durability means the lifetime and stability of fabrics made of fiber-based F-TEGs [105].

So far, many thermoelectric fibers with high flexibility and thermoelectric performance are made by combining the organic and inorganic materials, and these fibers are fabricated in a small laboratory scale rather than in the large scale natural environment, where toxic chemicals may be involved in the fabrication process of fibers [106]. It should be noted that conventional materials for fabrics are polyacrylonitrile (PAN) synthetic polymers [106], acetate [107], nylon [108], and polyester [109]. These materials are fabricated from toxic chemicals which are processed into the solution for the strands that can be woven into fabrics, which can seriously affect the healthy immune system of human, and also might bring environmental issues [110]. For example, it is reported that nylon, made from coal, petroleum, and natural gas, is a conventional material for fabrics, and its fabrics might cause breast cancer along with many other chronic illnesses [111]. Hence, the selection of materials for fiber-based F-TEGs is key to avoid the potential health problem and ethical issues in the future.

Durability is also a critical factor to evaluate the wearability of fiber-based F-TEGs. Thermoelectric fabrics should satisfy high resilience, high tensile strength, and high abrasion resistance. In addition, stain release, odor resistance, and colorfastness are also important factors in the design of

thermoelectric fabrics [112], as illustrated in **Figure 2(d)**. High resilience of fabrics is required because thermoelectric fabrics are expected to adhere to human skins all the time even though a massive stretch of fabrics exists. Heat harvesting can be more effective when this factor can be achieved [112]. Tensile strength means strength during the fabrication process. Fibers are expected to be twisted and bent multiple times and not to be broken during the fabrication process [112]. Abrasion resistance is commonly existed in most fabric applications, meaning resistance to friction caused by rubbing. Rubbing can be generated by the internal environment between skins and fabrics, and by the external environment between fabrics and surroundings. High abrasion resistance can ensure the rubbing cannot damage the fabric and then lead to the loss of the thermoelectric performance or flexibility [113]. Stain release can ensure thermoelectric fabrics washed to remove stains and ensure the lifetime of wearable capability. Odor resistance can appropriately deal with the relationship between fabrics and perspiration. High odor resistance can ensure the smell of fabrics in the long-term. Colorfastness is the factor that affects the presentation of the fiber-based F-TEGs. High colorfastness can avoid the fade of the fabrics when exposed to sunlight, and also promise a longer lifetime.

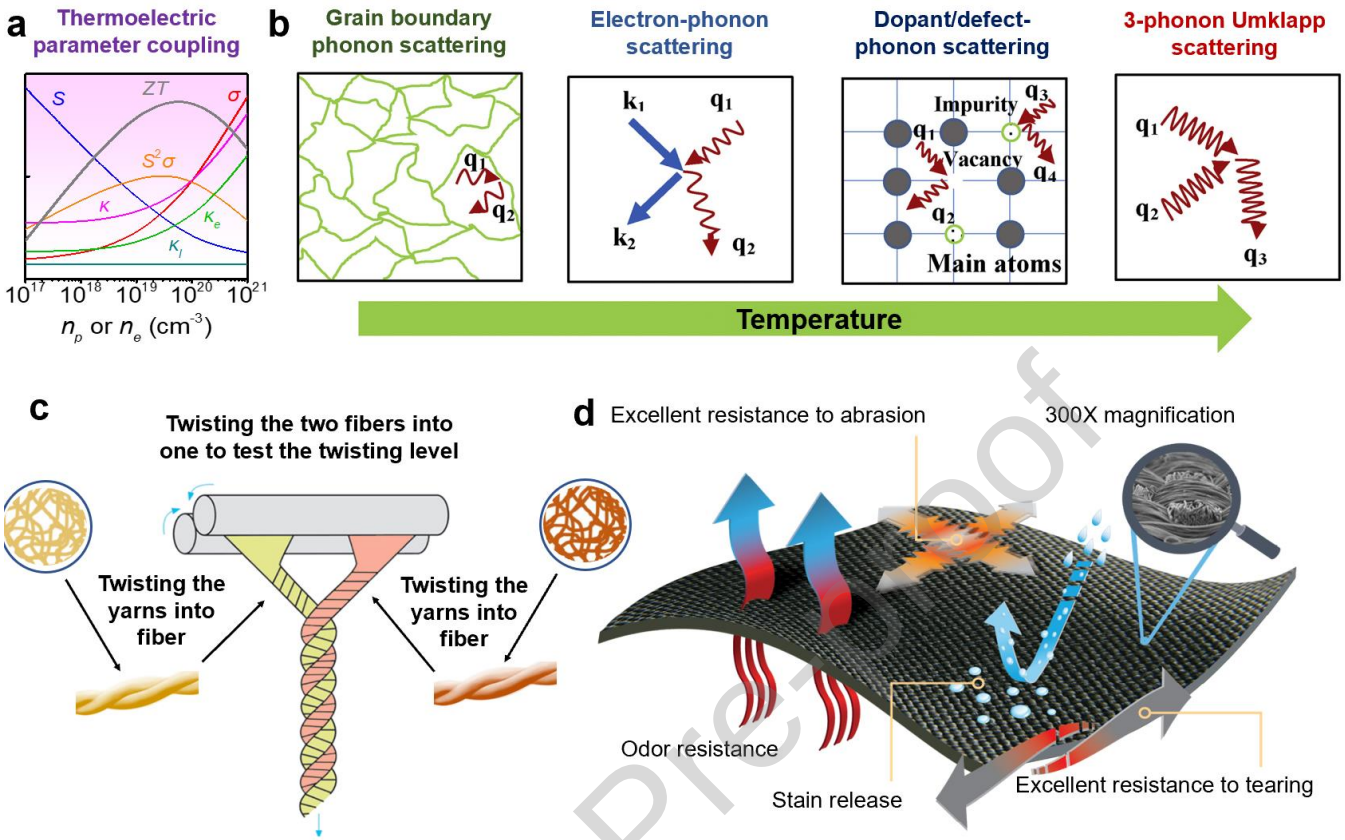

Figure 2. (a) Schematic diagram of parameter coupling in thermoelectric materials. (b) Schematic diagram of the phonon scattering mechanism. Reproduced with permission [100]. Copyright 2019 Elsevier. (c) Illustration of twisting the yarns into a fiber. **(d)** Illustration of the durability of fabrics. Reproduced from https://www.cordura.com/en/Fabrics/classic-fabric. Copyright 2020, INVISTA.

Fiber-based Thermoelectric Materials

Materials are core elements of fiber-based F-TEGs, so that the selection of appropriate materials is a critical factor for the design and fabrication of F-TEGs. Appropriate fiber-based materials should have high *ZT*s at low temperatures. To achieve this goal, high *S* and appropriate *n* and *μ* are required to promise high carrier transports. Mechanical and thermal properties, materials cost, and convenience of fabrication are also key factors for their scale-up production. Current progress on fiber-based inorganic

thermoelectric materials, organic thermoelectric materials, and hybrid thermoelectric materials are summarized in **Table 1**.

Table 1 Summary of thermoelectric performance of typical fiber-based thermoelectric materials. Here CNT is abbreviated from carbon nanotube, PPy is abbreviated from polypyrrole, P3HT is abbreviated from poly(3-hexylthiophene), CSA is abbreviated from camphorsulfonic acid, PEDOT is abbreviated from poly(3,4-ethylenedioxythiophene), PEDOT:PSS is abbreviated from poly(3,4-ethylenedioxythiophene):poly(styrenesulfonate), P3OT is abbreviated from poly(3-octylthiophene), PEDOT:Tos is abbreviated from poly(3,4-ethylenedioxythiophene) tosylate, PANI is abbreviated from polyaniline, PEG is abbreviated from poly(ethylene glycol), rGO is abbreviated from reduced graphene oxide, PVAc is abbreviated from polyvinyl acetate, PVDF is abbreviated from polyvinylidene fluoride, PTSA is abbreviated from p-toluenesulfonic acid, and PEI is abbreviated from polyethyleneimine.

Year	Sample	ZT	$S^2\sigma$ (μW m^{-1} K^{-2})	σ (S cm^{-1})	S (μV K^{-1})	κ (W m^{-1} K^{-1})	Ref.
Inorganic thermoelectric fiber							
2011	Recycled carbon fiber sheets	-	0.4	11.4	-19.36	-	[114]
2012	Recycled carbon fiber sheets + Bi_2Te_3	0.000966	32.2	112.4	-53.6	-	[80]
2012	PbTe-coated glass fiber	0.75	406.0	1.7	1545.3	0.262	[115]
2015	Ag_xTe_y nanofiber	-	4.0	6.8	-76.7	-	[116]
2016	Graphene fibers	0.00000374	1.9	1183.5	-3.9	140.7	[117]
2016	$Bi_{0.5}Sb_{1.5}Te_3$ fibers	-	260	69.8	193.0	-	[81]
2017	CNT-coated glass fiber	-	109.8	1800.0	24.7	-	[118]
2017	$Bi_{0.5}Sb_{1.5}Te_3$ core fiber	1.25	3529.0	1568.0	150.0	0.844	[82]
2018	Graphene fibers	0.00276	624	4864.0	38.2	86.6	[119]
2018	Recycled carbon fiber sheets + Bi_2Te_3	-	~0.2	1.2	-40	-	[120]

2018	Bi_2Se_3 core fiber	0.18	725.9	319.0	-150.9	1.25	[121]
2018	Bi_2Te_3 core fiber	0.73	1267.0	744.0	130.5	0.52	[83]
2018	Si nanotube fabrics	0.34	-	-	320.0	-	[122]
2019	Recycled carbon fiber + Bi_2Te_3 + CNT	-	~1.0	2.0	-72.2	-	[123]
2020	SnSe core fiber	2.0	531.2	56.4	306.9	0.25	[84]
Organic thermoelectric fiber							
2005	CSA-doped PANI fiber	-	1.13	67.9	12.9	-	[124]
2014	PPy nanotube film	0.000571	0.31	9.8	17.7	0.17	[125]
2014	P3HT nanofiber network	0.0026	6.75	-	-	-	[85]
2015	PEDOT nanofiber	-	16.4	71.4	48.0	-	[126]
2017	P3HT nanofiber mat	0.016	3.7	14.8	50	0.0708	[86]
2018	PEDOT:PSS fiber	-	4.7	175.2	16.4	-	[127]
2020	PEDOT:PSS fiber	0.09	147.8	4029.5	19.2	1.0	[87]
Hybrid thermoelectric fiber							
2012	CNT/PANI composite nanofiber	-	0.18	16.9	10.2	-	[128]
2013	Carbon fibers + epoxy + Te/Bi_2Te_3/carbon black	0.086	126.9	47.6	163.3	0.511	[88]
2014	Glass fabric + Bi_2Te_3	0.33	1029.3	549.2	-136.9	0.93	[89]
2014	Paper + PEDOT:PSS	0.0055	3.0	53.9	23.6	0.16	[129]
2015	Carbon fiber sheets + P3OT	-	7.1	3.9	134.5	-	[130]
2015	Cellulose fiber + CNT network	-	8.1	29.0	53.0	-	[131]
2015	Polyester fabric + PEDOT:PSS	-	0.04	1.5	16.3	-	[132]
2016	Sb_2Te_3 + PAN yarn	0.24	2376.3	750.0	178.0	3.0	[90]
2017	CNT/PEG composite thread	-	107.2	47.8	47.3	-	[133]
2017	Polyester fabric + graphite	-	0.065	0.5	35.0	-	[134]

2017	Cellulose fiber + PEDOT:PSS	0.0013	1.5	31.0	22.0	0.1	[135]
2017	Glass fabric + $Bi_2Te_{2.7}Se_{0.3}$	0.81	2077.3	763.0	-165.0	0.37	[91]
2018	CNT/PEDOT:PSS composite fiber	-	113.0	541.4	-45.7	-	[136]
2018	rGO + PPy nanotube hybrid film	-	7.3	81.0	30.0	-	[137]
2018	Cellulose fiber + Bi_2Te_3	0.38	377.5	209.6	-134.2	0.47	[92]
2018	Glass fiber coated by PEDOT:PTSA	-	6.74	31.8	48.5	-	[138]
2019	Carbon fibers + epoxy	-	245.0	1630.0	33.9	-	[139]
2019	Carbon nanofibers + lignin	-	0.01	27.5	2.0	-	[140]
2019	Cotton fabric + PEDOT:PSS	-	0.5	18.8	16.2	-	[141]
2019	Nylon membrane + Ag_2Se film	0.6	987.4	497.0	-140.0	0.478	[93]
2020	CNT yarn + PEI	-	667.8	1408.3	-68.7	-	[142]
2020	Ta_4SiTe_4 whisker + PVDF	-	1045.7	99.0	-325.0	-	[143]
2020	Te nanowire + PEDOT:PSS fiber	-	78.1	250.8	55.8	-	[144]
2020	Acrylic fiber-wrapped CNT yarn + PEDOT:PSS	-	346.2	949.0	60.4	-	[145]

3.1 Inorganic materials

A few semiconductors with high *ZT* values can be used as materials applied to F-TEGs. However, most of them are rigid and brittle, leading to difficulty fabricated as flexible fibers. Nevertheless, some advanced fabrication methods have been developed, including electrospinning [122, 146], wet spinning [147], and thermal drawing [148]. For example, inorganic $BaTiO_3$ fibers were fabricated using electrospinning from a prepared solution [146]. In such a prepared precursor solution, barium acetate was firstly dissolved in glacial acetic acid and then added titanium isopropoxide to form $BaTiO_3$

precursor solution. Also, a solvent solution of mixed the poly (vinyl pyrrolodone) (PVP), dimethyl formamide, and ethanol together were prepared. The solvent solution was added to the precursor solution to form the prepared solution for electrospinning. The as-fabricated $BaTiO_3$ fibers have an averaged diameter of ~170 nm, and fibrous geometry is well organized and assembled by fine-grained structures [146]. Similar works were reported in $SrTiO_3$-based fibers [149]. Another example is using wet-spinning to fabricate inorganic fibers. So far, the wet-spinning technique has been widely used to fabricate inorganic thermoelectric fibers, such as graphene fibers [117, 119, 150] and carbon nanotube (CNT) fibers [151]. Thermal drawing is also used to fabricate inorganic core fibers, such as p-type $Bi_{0.5}Sb_{1.5}Te_3$ and n-type Bi_2Se_3 core fibers [148].

Carbon-based thermoelectric fibers are important members of fiber-based thermoelectric materials, such as conventional carbon fibers and graphene fibers. Sometimes CNTs can also be treated as carbon fibers. **Figure 3(a)** summarizes the $S^2\sigma$ of some typical carbon-based thermoelectric fibers [117, 119, 152-173], and the inset shows a scanning electron microscopy (SEM) image of a section of typical graphene fiber [119]. Generally, rational doping and treatments can significantly improve the thermoelectric performance of thermoelectric carbon fibers [174]. It was reported that CNT papers treated with Ar plasma can exhibit a high ZT of 0.4 at 673 K, derived from the high $S^2\sigma$ of 120.5 μW m^{-1} K^{-2} and low κ of W m^{-1} K^{-1} [175]. In addition to carbon-based thermoelectric fibers, glass fibers coated with inorganic semiconductor nano/microcrystals are also typical inorganic thermoelectric fibers. **Figure 3(b)** shows a SEM image of PbTe-coated glass fibers [115]. The inset shows the coating composed of PbTe nanocrystals [115]. The fibers were fabricated through solution-phase deposition of PbTe nanocrystals onto glass fibers. The as-fabricated fibers possess a high ZT of 0.75 at 400 K, derived from the high $S^2\sigma$ of 406 μW m^{-1} K^{-2} and low κ of 0.226 W m^{-1} K^{-1} [115]. **Figure 3(c)** illustrates power

generation by harvesting heat from industrial pipes using such inorganic fiber-based F-TEGs [115], indicating great values for applying to industrial plants.

In terms of other types of inorganic thermoelectric fibers, **Figure 3(d)** shows a SEM image of Si-based thermoelectric fabric, fabricated by a typical electrospinning route [122]. The as-fabricated fabric possesses large-area and adaptable features. A high *ZT* of 0.34 at 823 K can be achieved in this advanced fabric, as shown in **Figure 3(e**) [122]. Much recently, a unique inorganic core fiber is developed. **Figure 3(f)** shows an optical image of SnSe core fibers, fabricated by a thermal drawing process [84]. By a post-draw laser recrystallization process, single-crystal SnSe core fibers can be achieved with a record high *ZT* of 2 at 862 K, as shown in **Figure 3(g)** [84]. Similarly, a high *ZT* of 1.25 was reported in $Bi_{0.5}Sb_{1.5}Te_3$ core fiber at 300 K [82], and a high *ZT* of 0.73 was reported in Bi_2Te_3 core fiber [83], both using the same fabrication routes. The achieved high thermoelectric properties are promising for applying to practical thermoelectric devices.

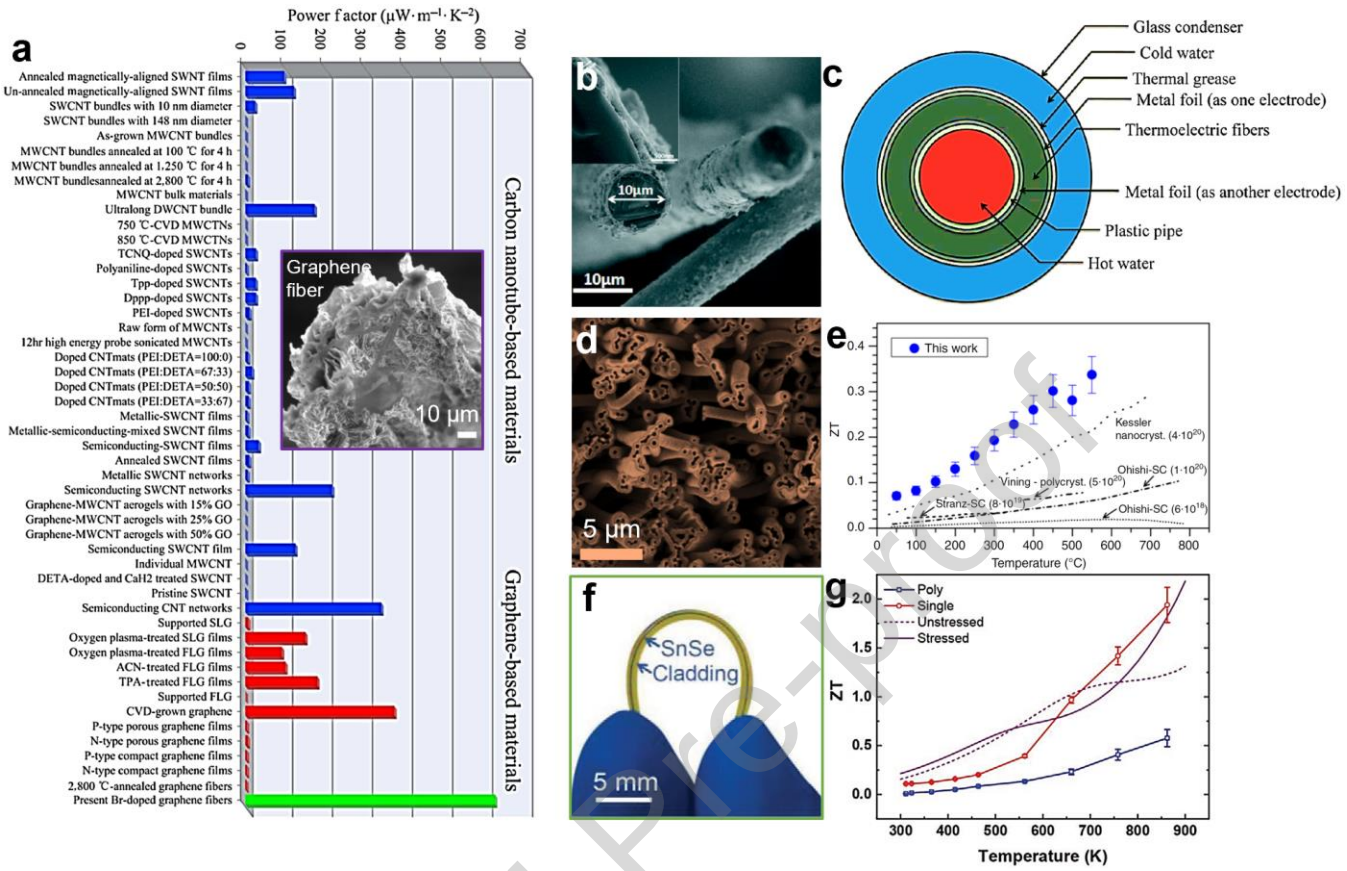

Figure 3. (a) Reported room-temperature power factors ($S^2\sigma$) of CNT- and graphene-based thermoelectric fibers. The inset shows a scanning electron microscopy (SEM) image of a section of typical graphene fiber. Reproduced with permission [119]. Copyright 2018 Springer Nature. (b) SEM image of PbTe-coated glass fibers. The inset shows the coating composed of PbTe nanocrystals. (c) Illustration of power generation using inorganic fiber-based F-TEGs realized by harvesting heat from industrial pipes. Reproduced with permission [115]. Copyright 2012 American Chemical Society. (d) SEM image of Si-based thermoelectric fabric. (e) Temperature-dependent *ZT* of the Si fabric. Reproduced under a Creative Commons Attribution 4.0 International License [122]. Copyright 2018 Springer Nature. (f) Optical image of SnSe core fibers. (g) Temperature-dependent *ZT* of SnSe core fibers. Reproduced with permission [84]. Copyright 2020 Wiley-VCH.

3.2 Organic materials

Organic thermoelectric materials are key materials for fabricating fiber-based F-TEGs due to their high flexibility and suitable thermoelectric properties. Some fabrication methods of organic thermoelectric fibers are similar to those of inorganic thermoelectric fibers, such as electrospinning [176] and wet-spinning [177]. Electrospinning is commonly used to fabricate polyaniline (PANI) fibers, while some organic acids can be added into PANI solution to enhance the solubility of PANI. It has been reported that camphoric acid (CSA) can be mixed with PANI, and then doped PANI, and polyethylene oxide (PEO) can be electro-spun into side-by-side bicomponent fibers [176]. The relative electrical resistance of PANI fibers is increasing with increasing the strain, in which the materials are more sensitive to the stretching rather than temperature [176]. Therefore, PEO/PANI fibers are more suitable for wearable sensors. In terms of wet-spinning, it is commonly used to fabricate poly(3,4-ethylenedioxythiophene):poly(styrene sulfonate) (PEDOT:PSS) fibers, as illustrated in **Figure 4(a)** [178]. This method involves the fabrication of a PEDOT:PSS aqueous solution, loading the solution into the syringe, spinning the solution into the H_2SO_4 coagulation bath, and post-treating the obtained fibers to improve their thermoelectric performance, as shown in **Figure 4(b)** [177]. **Figure 4(c)** shows a SEM image of as-fabricated PEDOT:PSS fibers after H_2SO_4 treatment [177]. The rational post-treatment can further improve the electrical transport performance of PEDOT:PSS [179, 180]. **Figure 4(d)** shows the thermoelectric performance of the as-fabricated PEDOT:PSS fiber as a function of needle diameter [87]. The results indicate that a rational dimension is also important to optimize the thermoelectric performance. In addition to the thermoelectric performance, organic fiber also exhibits excellent mechanical properties. **Figure 4(e)** shows the mechanical properties of PEDOT:PSS fiber as a function of strain at break [87]. It is seen that the treated fiber exhibits a high tensile strength of 375 MPa, which is especially suitable for applying to wearable F-TEGs.

In some situations, the as-fabricated organic fibers possess unique structures. **Figure 4(f)** shows an optical image of PEDOT:PSS fibers using traditional wet spinning technique [177], and **Figure 4(g)** shows a SEM image of as-fabricated PEDOT:PSS fibers [177], which have a hollow structure. The hollow structures can be affected by the spinning speed, needles, and temperature in the drying process. Such a hollow structure increases surface area and effectively reduce the insulating PSS and in turn enhance thermoelectric performance [177]. The S can be estimated to be ~24 $\mu V\ K^{-1}$ [177]. **Figure 4(h)** illustrates fabricating and evaluating PEDOT:PSS fiber-based sensors [177]. The sensors are composed of PEDOT:PSS fibers with different numbers, polyvinylidene fluoride (PVDF) substrates, and Cu wires as connectors [177]. **Figure 4(i)** shows the output of the 5 different sensors with different numbers of fibers at a ΔT of 6 K [177]. With increasing the number of applied fibers, the voltage triggered by human fingers is significantly enhanced, indicating successful designed sensors to detect the temperature change. Therefore, organic thermoelectric fibers possess significant potential for applying to various applications.

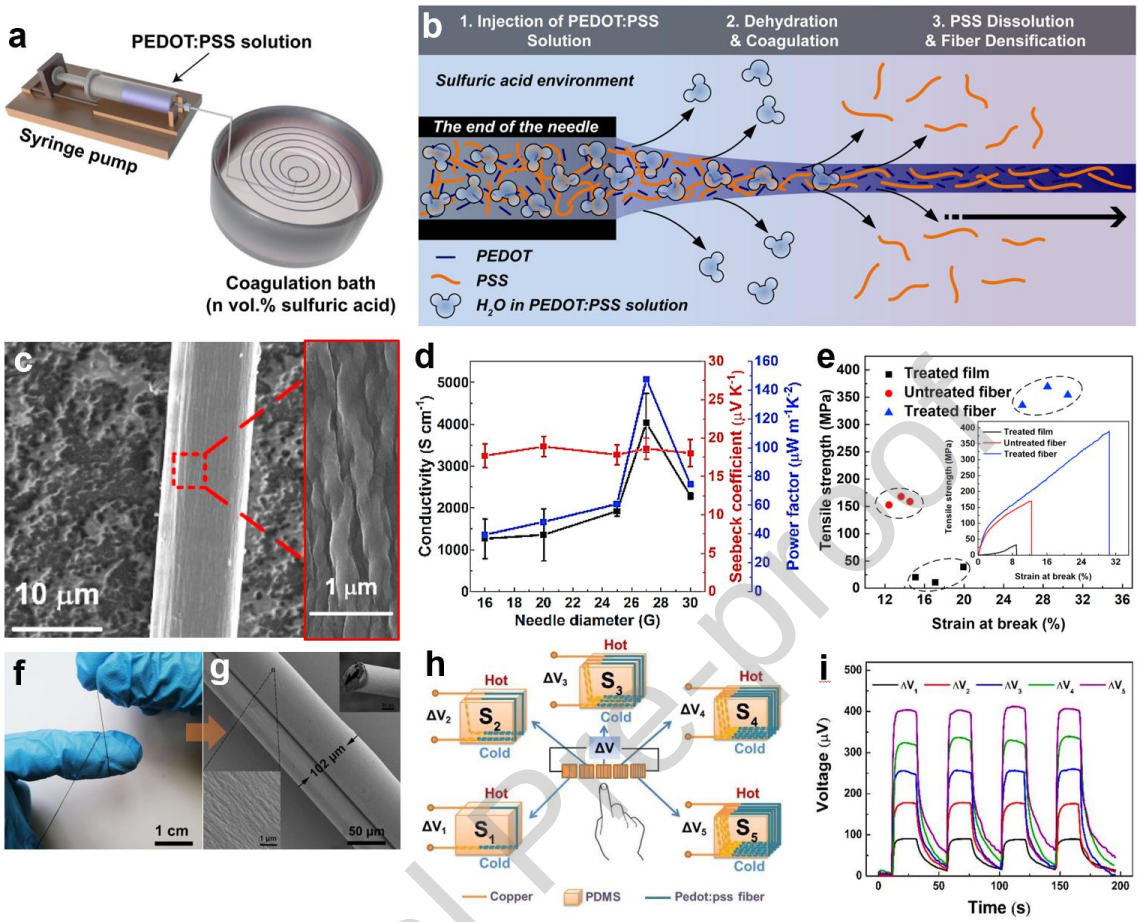

Figure 4. (a) Schematic diagram of fabricating PEDOT:PSS fibers by wet-spinning. (b) Mechanism for PEDOT:PSS microfiber formation in an acidic coagulation bath. Reproduced under a Creative Commons Attribution 4.0 International License [178]. Copyright 2018 Springer Nature. (c) SEM images of a PEDOT:PSS fiber after H_2SO_4 treatment. (d) The thermoelectric performance of PEDOT:PSS fiber as a function of needle diameter. (e) The mechanical properties of PEDOT:PSS fiber as a function of strain at break. Reproduced with permission [87]. Copyright 2020 Elsevier. (f) Optical and (g) SEM images of hollow PEDOT:PSS fiber. (h) Illustration of fabricating and evaluating PEDOT:PSS fiber-based sensors. (i) Output of the 5 different sensors. Reproduced under the Creative Commons Attribution License [177]. Copyright 2020 MDPI.

3.3 Hybrid materials

Hybrid materials, which combine inorganic materials and organic polymers, exhibit both good thermoelectric properties and high flexibility [116]. By combining the organic matrix with inorganic fillers, the advantage of inorganic materials (such as high S and high σ) and the advantage of polymers (such as low κ and high flexibility) maintain to a great extent. To realize such unique hybrids, one general method is to coat inorganic materials on the organic substrates. However, the coating may also affect the flexibility of organic materials or thermoelectric properties of inorganic materials. For example, p-type $Bi_{0.5}Sb_{1.5}Te_3$ and n-type $Bi_2Te_{2.7}Se_{0.3}$ can mix with binders and organic solvent to form printing inks. Such printing inks can be screen-printed on any organic flexible fibers [91]. The particles after the screen-printing have a size range of 1-20 μm [91]. The as-printed thermoelectric layers showed a high ZT of 0.65 in p-type $Bi_{0.5}Sb_{1.5}Te_3$ based hybrid and a high ZT of 0.81 in n-type $Bi_2Te_{2.7}Se_{0.3}$ based hybrid [91]. In another example, a distilled PEDOT was first prepared and mixed with p-toluenesulfonic acid (p-TSA) solution, then immersed the glass fiber into the solution and dried in the vacuum oven to form the PEDOT:p-TSA/glass fiber [138]. By the solution-based coating, particles of the polymers are agglomerated on the glass fibers, and the particles are formed from the self-curly polymer chains, indicating the van der Waals force existed between the particles, leading to a higher thermoelectric performance [138]. With the addition of the oxidant ammonium peroxydisulfate (APS), the maximum S and σ have reached 32 μV K^{-1} and 169 S cm^{-1}, respectively, leading to a $S^2\sigma$ of 6.74 μW m^{-1} K^{-2} [138].

In addition to simply coating inorganic materials on organic substrates, there are also some other routes to rationally mix the organic and inorganic materials. To illustrate, **Figure 5(a)** shows a SEM image of the Ag_2Se nanofibers, fabricated by a typical solution method [93]. These Ag_2Se nanofibers were then uniformly dispersed in ethanol, and the solution was vacuum filtrated on a nylon membrane. After a hot-pressing process, a Ag_2Se film was achieved, as shown in the SEM image in **Figure 5(b)**

[93]. **Figure 5(c)** shows the thermoelectric properties of the Ag_2Se film as a function of temperature [93]. A high $S^2\sigma$ of ~987.4 μW m^{-1} K^{-2} was achieved at 300 K, along with excellent flexibility. The σ was only reduced by 7 % after 1000 bending cycles around an 8-mm diameter rod, indicating great flexibility [93]. In addition to the vacuum filtration and hot-pressing routes, an unbalanced magnetron sputtering technique was also reported to combine Bi_2Te_3 thick film with ubiquitous cellulose fibers. **Figure 5(d)** and **5(e)** show SEM images of side and top views of the as-fabricated Bi_2Te_3/cellulose fiber composite material [92], in which the fibers are well distributed in Bi_2Te_3 matrix. Such a unique material possesses hierarchical porous structures, which significantly affect the electrical and thermal transports, as illustrated in **Figure 5(f)** [92]. **Figure 5(g)** shows the temperature-dependent *ZT* of the composite, from which a high *ZT* of ~0.4 can be achieved at 480 K [92]. Furthermore, **Figure 5(h)** shows a schematic diagram of the flexible PVDF/Ta_4SiTe_4 whisker composite film [143], fabricated by a solution-based route. The Ta_4SiTe_4 as inorganic fillers were fabricated by a chemical vapor transportation method. **Figure 5(i)** shows the microstructure of the composite film, while **Figure 5(j)** shows SEM and optical images of the composite film [143]. Benefited from the flexible feature of PVDF and well-distributed Ta_4SiTe_4 whisker in the PVDF, the as-fabricated composite film exhibits high flexibility. **Figure 5(k)** shows the thermoelectric properties of the composite film as a function of temperature [143]. A high $S^2\sigma$ of 1050 μW m^{-1} K^{-2} could be achieved at 200 K, derived from the high S of ~-325 μV K^{-1} [143]. Such a high thermoelectric performance with good flexibility exhibits great potential for applying to wearable F-TEGs.

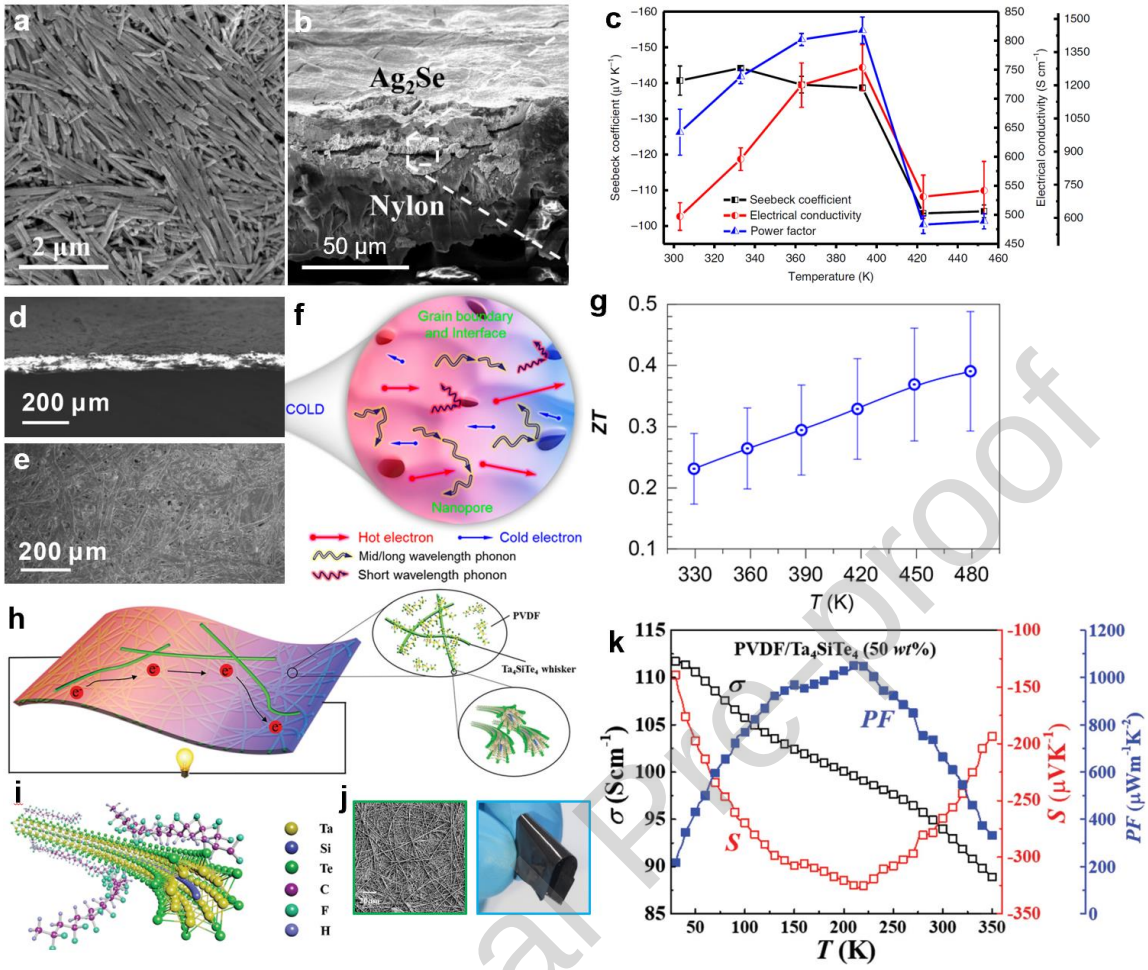

Figure 5. (a) SEM image of the Ag_2Se nanofibers. (b) SEM image of hot-pressed Ag_2Se film on a nylon membrane. (c) Thermoelectric properties of the Ag_2Se film as a function of temperature. Reproduced under a Creative Commons Attribution 4.0 International License [93]. Copyright 2019 Springer Nature. SEM images of (d) side and (e) top views of Bi_2Te_3/cellulose fiber composite material. (f) Illustration of electron and phonon transport in the composite. (g) Temperature-dependent *ZT* of the composite. Reproduced with permission [92]. Copyright 2018 American Chemical Society. (h) Schematic diagram of the flexible PVDF/Ta_4SiTe_4 whisker composite film. (i) The microstructure of the composite film. (j) SEM (left) and optical (right) images of the composite film. (k) Thermoelectric properties of the composite film as a function of temperature. Reproduced with permission [143]. Copyright 2020 Royal Society of Chemistry.

The flexible organic matrix can significantly affect the thermoelectric properties of hybrid materials. Therefore, various methods, such as doping and de-doping [102], post-treatment [179-181], crystallinity and alignment [182], have been explored to improve thermoelectric performance of flexible organic matrix, mainly conducting polymers.

Doping and De-doping. Chemicals such as dimethyl sulfoxide, tetrahydrofuran, and KOH are widely used as dopants to tune μ, n, and oxidation level of conducting polymers to enhance σ and S [183]. Particularly, suitable dopants can effectively increase μ for several orders of magnitude in conducting polymers. The enhanced μ is attributed to the fact that these dopants can re-orient the chain between the conducting polymers [184]. Moreover, the chain of conducting polymers can be further enhanced after de-doping [185]. For example, a ZT of 0.25 was obtained in tosylate-doped PEDOT:PSS [186] and KOH de-doped PEDOT:PSS showed an enhanced S from 15 μV K^{-1} to 90 μV K^{-1} [187].

Post-treatment. Conformation and oxidation level of conducting polymers can be tuned by post-treatments [181]. Post-treatments contain immersing conducting polymers in various solvents and organic solutions with inorganic salts [188-190]. For example, immersing PEDOT:PSS into the ethylene glycol solvent can enhance its ZT [191]. After immersing in ethylene glycol, non-complexed PSS chains of PEDOT:PSS films can be removed leading to an enhanced ZT of 0.42 in PEDOT:PSS [102]. Changing the conformation of conducting polymers can enhance σ. Structures of PEDOT:PSS can be rearranged by the H_2SO_4 post-treatment, leading to higher σ. As a result, the $S^2\sigma$ of H_2SO_4 post-treatment PEDOT:PSS may reach ~17 μW m^{-1} K^{-2}, which is significantly higher than that of pristine PEDOT:PSS (0.006 μW m^{-1} K^{-2}) [192]. In addition, the highest $S^2\sigma$ of 334 μW m^{-1} K^{-2} was reported in PEDOT:PSS treated by H_2SO_4 and NaOH [190]. These positive results indicate the combination of acid and base treatment can effectively increase σ and the oxidation levels of conducting polymers [188]. Recent,

immersing PEDOT:PSS in N,N-dimethylformamide (DMF) solution of $ZnCl_2$ was reported, from which an enhanced S of 26.1 μV K^{-1} and $S^2\sigma$ of 98.2 μW m^{-1} K^{-2} were achieved [193].

Crystallinity and Alignment. Carriers in conducting polymers have two types of transport methods. One is along the conducting polymer chain, and the other is hopping between the interchain. Generally, μ along the chain is normally higher than that of hopping [77]. Hence, increasing the crystallinity and chain alignment of conducting polymers can be used to tune their thermoelectric properties [194]. Single-crystalline PEDOT nanowires, can be fabricated by using the direct printing and vapor phase polymerization, and the results showed that the product has high crystallinity and an ultrahigh σ of 8000 S cm^{-1} can be achieved [195], attributed to the single-crystalline structures of PEDOT nanowires. In addition, stretching is also an appropriate method to enhance σ of concocting polymers. After stretching by 5-fold, the σ of I-doped polyacetylene still exhibited a value of 10^5 S cm^{-1} [196].

Fiber-based Thermoelectric Devices and Applications

4.1 Device structure and performance

Based on their dimensions, fiber-based F-TEGs can be classified into one-dimensional (1D), two-dimensional (2D), and three-dimensional (3D) structures. The 1D structure is based on yarns, filaments, or fibers. The 2D structure is based on films composed of fibers embedded on the surface of flexible substrates; and the 3D structure is to assemble 1D thermoelectric yarn/filament/fiber into textiles [82]. **Table 2** summarizes the current fiber-based F-TEGs and their power output.

Table 2 Summary of materials and thermoelectric output of typical fiber-based F-TEGs. Here DPPP is abbreviated from 1,3-bis(diphenylphosphino)propane, PEIE is abbreviated from polyethyleneimine ethoxylated, and [BMIM]PF_6 is abbreviated from 1-butyl-3-methylimidazolium hexafluorophosphate.

Year	Materials p-type	n-type	Couple number	ΔT (K)	Output voltage (mV)	Output power (μW)	Ref.
2008	Ni–Ag-coated silica fiber	-	7	6.6	0.9	0.002	[197]
2013	-	Polyester fabric + Bi_2Te_3	20	30	25.0	2.1	[198]
2014	Glass fabric + Sb_2Te_3	Glass fabric + Bi_2Te_3	8	50	90.0	-	[89]
2014	Polymer fabric + $Bi_{0.5}Sb_{1.5}Te_3$	Polymer fabric + $Bi_2Se_{0.3}Te_{2.7}$	12	15	25.0	0.224	[199]
2015	Polyester fabric + PEDOT:PSS	Ag wire	5	75.2	4.3	0.0125	[132]
2015	Cellulose fiber + CNT network	Cellulose fiber + CNT network treated with PEI	5	50	16.8	0.0755	[131]
2015	Nylon fiber + PEDOT:PSS	Nylon fiber + Ag_2Te	-	20	-	0.005	[200]
2016	$Bi_{0.5}Sb_{1.5}Te_3$ fiber	$Bi_2Te_{2.7}Se_{0.3}$ fiber	2	12	4.8	0.018	[81]
2016	Silk fabric + Sb_2Te_3	Silk fabric + Bi_2Te_3	12	35	10.0	0.015	[201]
2017	CNT yarn doped by $FeCl_3$	CNT yarn	240	40	46.7	4.1	[202]
2017	Sb_2Te_3 + PAN yarn	Bi_2Te_3 + PAN yarn	-	200	-	14.2	[90]
2017	CNT/PEG composite thread	CNT/PEG composite thread doped with $[BMIM]PF_6$	-	25	-	0.008	[133]
2017	$Bi_{0.5}Sb_{1.5}Te_3$ core fiber	Bi_2Se_3 core fiber	7	60	97.0	-	[82]
2017	Cellulose fiber + PEDOT:PSS	Ni foil	6	48.5	6.0	2.4	[135]
2018	Si nanotube fabric	-	-	70	22.0	-	[122]
2018	Cellulose fiber + $(Bi,Sb)_2Te_3$	Cellulose fiber + Bi_2Te_3	12	50	144.0	-	[92]

2018	PEDOT:PSS fiber	CNT fiber	5	60	20.7	-	[127]
2018	CNT + PEDOT:PSS composite fiber treated with hydrazine	CNT + PEDOT:PSS composite fiber treated with PEI	12	10	8.0	0.43	[136]
2018	Cotton thread + P3HT	Cotton thread + Ag paste	13	50	12.0	1.15	[203]
2019	Carbon fiber + epoxy	-	-	75	19.6	0.87	[139]
2019	CNT fiber	CNT fiber doped by DPPP	40	20	56.5	2.0	[151]
2019	Cotton fabric + PEDOT:PSS	CNT fiber	8	60	45.0	375.0	[141]
2019	Graphene oxide fiber	Graphene oxide fibers treated with PEIE	4	70	3.0	0.5	[150]
2019	Commercial textile coated by PEDOT	CNT fiber	5	100	21.0	0	[204]
2019	-	Nylon membrane with Ag_2Se film	4	30	18.0	0.46	[93]
2020	PEDOT:PSS fiber	Ni wire	5	9.1	1.9	-	[87]
2020	Hollow PEDOT:PSS fiber	-	5	6	0.4	-	[177]
2020	CNT yarn + PEDOT:PSS	CNT yarn + PEI	966	47.5	-	382.8	[142]
2020	Ta_4SiTe_4 whisker + PVDF	-	-	35.5	35.0	1.7	[143]
2020	Te nanowire + PEDOT:PSS fiber	Te nanowire + PEDOT:PSS fiber coated by Ag	28	40	25.9	0.2	[144]
2020	Acrylic fiber-wrapped CNT yarn with PEDOT:PSS	Acrylic fiber-wrapped CNT yarn doped by oleamine	15	44	43.5	4.38	[145]

1D Devices. With high flexibility, yarns, filaments, and fibers can be used to fabricate various textiles. Such units can be directly used to assemble 1D fiber-based F-TEGs, and/or as the building block for fabricating 2D and 3D fiber-based F-TEGs by weaving, knitting, stitching, braiding, and felting. For 1D devices, to ensure high thermoelectric output and flexibility, the p- and n-type thermoelectric materials are deposited on various fibers with promising flexibility [76]. To illustrate, taking inorganic thermoelectric fibers for examples, glass fibers can be coated by Al-doped ZnO to form p- and n-type junctions with a bare part, allowing a maximum Seebeck voltage of 1057.8 μV at a ΔT of 4.5 K [205]. Bi_2Te_3-based powders can be dissolved into an organic solvent with a thermoplastic resin to form fibers, which have similar S as their Bi_2Te_3-based bulks [81]. A maximum power output of a uni-couple reached ~10 nW, as shown in **Figure 6(a)**, although the higher power output can be achieved when more couples were connected in series or parallel [81]. Coating inorganic thermoelectric materials on the surface of carbon fibers can also obtain high power output. For example, Bi_2Te_3 coated carbon fibers by using the electro-deposition technique have S of -54 μV K^{-1}, which is higher than most organic materials [80]. It should be noted that the power output of as-prepared inorganic-fiber-based TEGs is still relatively low because fibers have high electrical resistances, attributed to their residual porosities and grain boundary contaminations. Therefore, future development should focus on reducing the electrical resistance and fundamental understanding of the relationship between grain boundary and electrical resistivity to increase power output [81].

In terms of the organic-fiber-based F-TEGs, the wet-spinning technique is commonly used to fabricate 1D fiber-based organic F-TEGs. Organic thermoelectric fibers can be prepared by dissolving the conducting polymers into a solvent and then solidifying in a coagulation bath. Kim *et al* prepared a 10 cm long semi-crystalline *via* dissolving an aqueous PEDOT:PSS in an aqueous sulfuric acid [206]. **Figure 6(b)** is a schematic illustration for PEDOT:PSS fiber embroidered thermoelectric module

consisting of ten elements (each comprising one p-type PEDOT:PSS fiber and one silver-plated nylon yarn). The PEDOT:PSS fibers and Ag-plated nylon yarns are embedded into the conventional fabric to form F-TEGs [206]. As shown in **Figure 6(b)**, the voltage and power can reach 8 mV and 2.6 nW at a ΔT of 40 °C, and its σ was not impacted by the deformation and bending [206]. It should be noted that, although the preparation and performance of 1D fiber-based organic F-TEGs have been developed rapidly, there are still issues to be solved, such as the relatively low performance and stability. Nevertheless, 1D fiber-based organic F-TEGs have significant potential to be integrated as a higher dimensional structures, but their thermoelectric performance may be affected when fiber-based organic F-TEGs are assembled.

To simultaneously realize good thermoelectric output and flexibility, 1D F-TEGs composed of inorganic/organic hybrid thermoelectric fibers are explored. To illustrate, **Figure 6(c)** shows an optical image and thermoelectric output of the TEG composed of wet-spun CNT/PEDOT:PSS hybrid fibers [136]. Under a ΔT of 10 °C, an output voltage of 8 mV, as well as an output power of ~450 nW, could be achieved. To further improve the thermoelectric output of hybrid-fiber-based 1D F-TEGs, various techniques are developed. **Figure 6(d)** illustrates the fabricating of highly integrable Te nanowire/PEDOT:PSS hybrid fibers and their application for wearable F-TEG [144]. Such composite fibers were fabricated by a conventional wet-spinning technique. To form p-n couples, the silver paste was coated at equal intervals on the fibers using a mask. The as-fabricated F-TEGs exhibit high mass-specific power of 9.48 μW g^{-1}, excellent mechanical flexibility, and superior integrability [144]. Similarly, **Figure 6(e)** shows an optical image and schematics of the CNT fiber-based TEG with a power measurement system [151]. The p-type CNT fibers were wet-spun from a 20 mg mL^{-1} CNT suspension in CSA and coagulated in ether and wrapped on a polydimethylsiloxane (PDMS) mold [151]. After that, one side of the materials was treated by chemical doping using 1,3-

bis(diphenylphosphino)propane (dppp) solution to become n-type, forming p-n couples [151]. The as-prepared F-TEG based on 40 pairs of p- and n-type CNT fibers shows the maximum power density of 259 μW g^{-1} at a Δ*T* of 20 K [151].

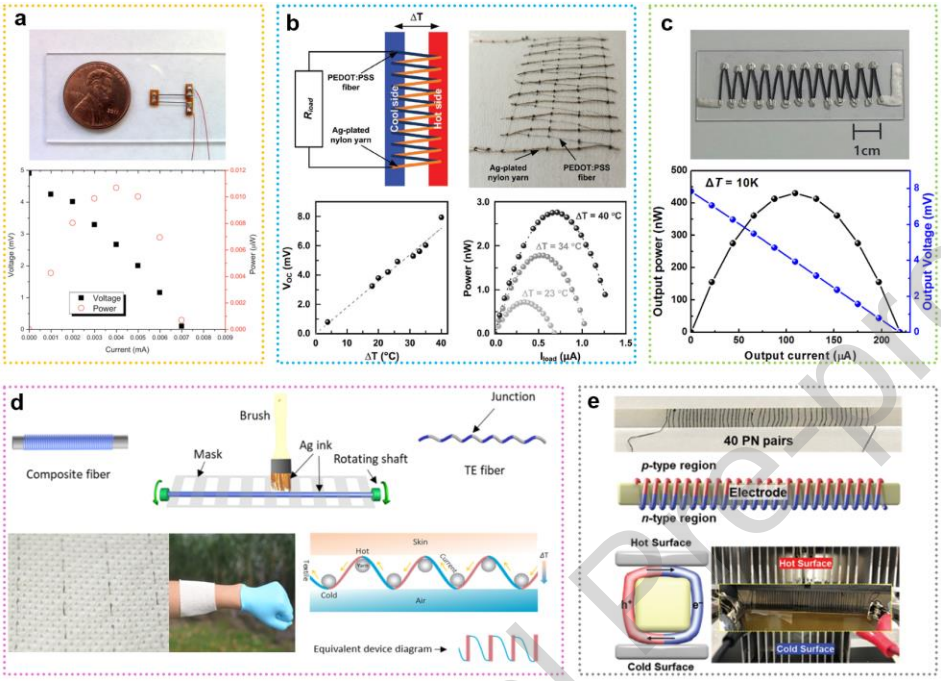

Figure 6. (a) Optical image and thermoelectric output of Bi_2Te_3 fiber-based miniature device by a Δ*T* of 12 K. Reproduced with permission [81]. Copyright 2015 Springer Nature. (b) PEDOT:PSS-fiber-embroidered thermoelectric module and its output voltage and power under different Δ*T*s. Reproduced under the terms of the Creative Commons CC BY license [206]. Copyright 2020 Wiley-VCH. (c) Optical image and thermoelectric output of the TEG composed of wet-spun CNT/PEDOT:PSS fibers. Reproduced with permission [136]. Copyright 2018 Elsevier. (d) Illustration of fabricating highly integrable Te nanowire/PEDOT:PSS hybrid fibers and their application for wearable F-TEG. Reproduced with permission [144]. Copyright 2020 American Chemical Society. (e) Optical image and schematics of the CNT fiber-based TEG with a power measurement system. Reproduced with permission [151]. Copyright 2019 Royal Society of Chemistry.

2D Devices. 2D structures are based on conventional fabrics, such as silk, cotton, nylon-based knitted, woven, and nonwoven fabrics. In the past several years, most of the development of 2D fiber-based F-TEGs has been focused on the preparation of thin-films made of fabrics. However, many issues are still existed, including lack of comfortability, poor deformability, and low damage tolerance [76]. To solve these issues, embedded and infiltrated methods are used to combine inorganic materials with high σ with textiles [2]. For example, 2D fiber-based F-TEGs were prepared by screen-printing techniques to coat the thermoelectric elements made by Bi_2Te_3 and Sb_2Te_3 on the woven fabric, which has shown excellent flexibility [89]. When the as-prepared device was bent with a 20 mm radius or 120 cycles of repeated bending with a 50 mm radius, high stability was maintained, and an impressive output power of 3.8 Wcm^{-2} was secured [89]. A similar study of Bi_2Te_3 and Sb_2Te_3 fabricated on the silk fabric showed an output power of 15 nW at a temperature difference of 35 K [201], the design of such unique 2D F-TEG is shown in **Figure 7(a)** [201], and its application as wearable F-TEG is shown in **Figure 7(b)** [201], respectively. Furthermore, **Figure 7(c)** shows top and side views of a polymer-based fabric printed by $Bi_{0.5}Sb_{1.5}Te_3$ and $Bi_2Se_{0.3}Te_{2.7}$ as thermoelectric units [199]. The F-TEG consisted of 12 thermocouples, connected by a conductive thread over an area of 6 × 25 mm^2 [199]. A power of 224 nW can be generated by the as-fabricated device for a ΔT of 15 K [199]. When the TEG was used on the human body, the measured output power was 224 nW at an ambient temperature of 5 °C [199]. The stability of such devices was further tested under multiple times of bending and stretching. Results indicated that the appropriate fabrication methods can lead the inorganic materials to be also wearable in clothing applications with high and stable power output [199]. It should be noted that there are still some limitations for the embedded method, especially for the lack of comfortability for the wearable devices due to the hardness and impermeability of the embedded fiber-based F-TEGs.

By weaving, knitting, braiding or mixing, 1D fibers can be interconnected to form 2D thermocouples [207]. For example, **Figure 7(d)** illustrates the fabricating carbon-fiber-based TEG and its thermoelectric output [139]. The as-designed F-TEG is a typical carbon-fiber-based thermoelectric generator, integrated as a lamina within an 8-ply laminate epoxy composite, and the fundamental thermoelectric unit is the carbon fiber reinforced polymer composite tow. The TEG laminate exhibited an output voltage of 19.56 mV and an output power of ~0.9 μW at a ΔT of 75 °C [139]. In addition, 2D fiber-based TEGs were fabricated by immersing commercial fabrics into PEDOT:PSS aqueous suspension and then cut fabrics into strips. Subsequently, strips were weaved on uncoated fabrics and connected with thin wires, as illustrated in **Figure 7(e)** [132]. The results show an output power of 12.29 nW at a ΔT of 75.2 K from 5 pieces of fabric strips [132], as shown in **Figure 7(e)**. Furthermore, Du *et al* use this method on other fabric strips containing cotton (p-type) and constantan wires (n-type), from which they obtained a voltage output of 18 mV and a maximum power of 212.6 nW at a ΔT of 75 K [208]. Other methods such as ultrasonication are used to coat PANI/CNT composites onto polyester fabrics. Fiber-based TEGs fabricated from two PANI/CNT composite-coated fabric strips showed an output power of 47 nW at a ΔT of 75 K [209].

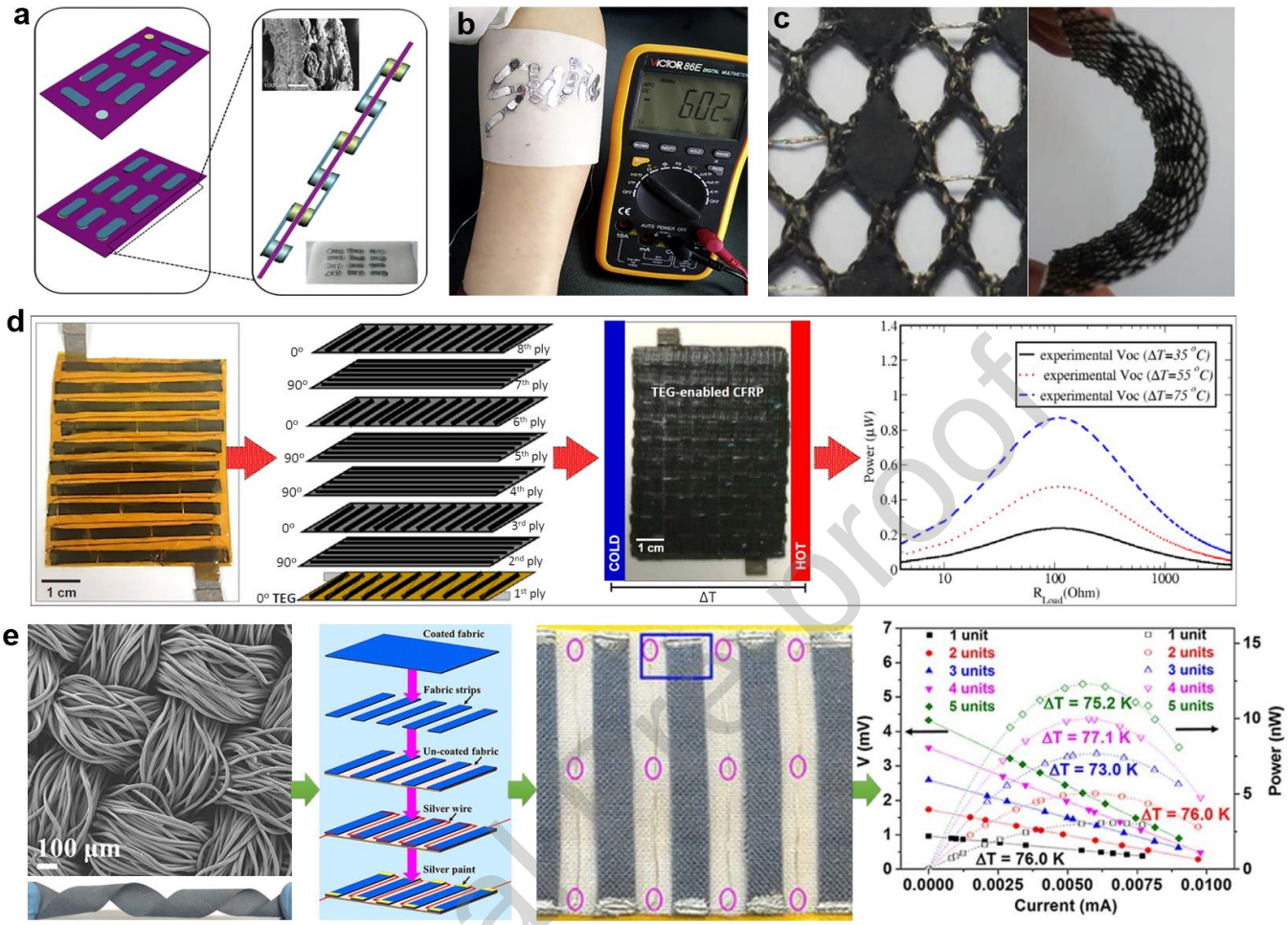

Figure 7. (a) Schematic diagram of fabricating silk fabric-based wearable F-TEG with inorganic nanostructured Bi_2Te_3 and Sb_2Te_3 as n-p thermoelectric units. (b) Illustration of the F-TEG used for power generation by harvesting heat from the human arm. Reproduced with permission [201]. Copyright 2016 Elsevier. (c) Top and side views of a polymer-based fabric printed by $Bi_{0.5}Sb_{1.5}Te_3$ and $Bi_2Se_{0.3}Te_{2.7}$ as thermoelectric units. Reproduced with permission [199]. Copyright 2014 IOP Publishing. (d) Illustration of fabricating carbon-fiber-based TEG and its thermoelectric output. Reproduced with permission [139]. Copyright 2019 Elsevier. (e) Illustration of fabricating F-TEG by PEDOT:PSS-coated commercial fabric and its thermoelectric output. Reproduced under a Creative Commons Attribution-NonCommercial-ShareAlike 4.0 International License [132]. Copyright 2015 Springer Nature.

3D Devices. 3D fiber-based F-TEGs are made of thermoelectric yarns/filaments/fibers, and can effectively collect heat energy due to the vertical temperature difference between the human body and surroundings. In addition, 3D fiber-based F-TEGs have better flexibility and heat-moisture comfortability. Therefore, 3D fiber-based F-TEGs are promising candidates for practical applications compared with 1D and 2D fiber-based F-TEGs [148].

Figure 8(a) shows an optical image of thermoelectric yarn with a $(Au/Bi_2Te_3/Au/Sb_2Te_3)n$ structure, made by electrospinning process that made PAN nanofiber sheets for conversion into a yarn [90]. The p-type Sb_2Te_3 and n-type Bi_2Te_3 were investigated in detail with different weave methods containing zigzag-stitch, garter-stitch, and plain-weave F-TEGs [90], and **Figure 8(b)** shows the optical image of plain-weave fiber-based F-TEGs [90]. Plain-weave fiber-based F-TEGs present the highest power output of 1.01 μW per couple at a temperature difference of 55 K, as shown in **Figure 8(c)**. Moreover, these 3D fiber-based F-TEGs were sensitive to the temperature difference, which means the power output could increase largely with the increase of temperature difference. Sun and his coworker developed the weave method and applied the interlocked thermoelectric loop to enable sufficient alignment with the heat flow direction, as illustrated in **Figure 8(d)** [145]. **Figure 8(e)** shows the optical images of the as-fabricated thermoelectric textiles [145]. To evaluate the flexibility and stretchability, **Figure 8(f)** shows photographs of the top view and schematic and infrared thermal image of thermoelectric textile after longitudinal stretching by 80 % [145], indicating excellent stretchability. Such a high mechanical property is suitable for applying to wearable F-TEGs. **Figure 8(g)** illustrates the methods for evaluating the thermoelectric output of the as-fabricated thermoelectric textile, and **Figure 8(h)** shows the output voltage and power of 3D fiber-based F-TEGs with different ΔTs. A power density of 70 mW m^{-2} is observed at a temperature difference of 44 K, which is much higher than other organic fiber-based F-TEGs [145].

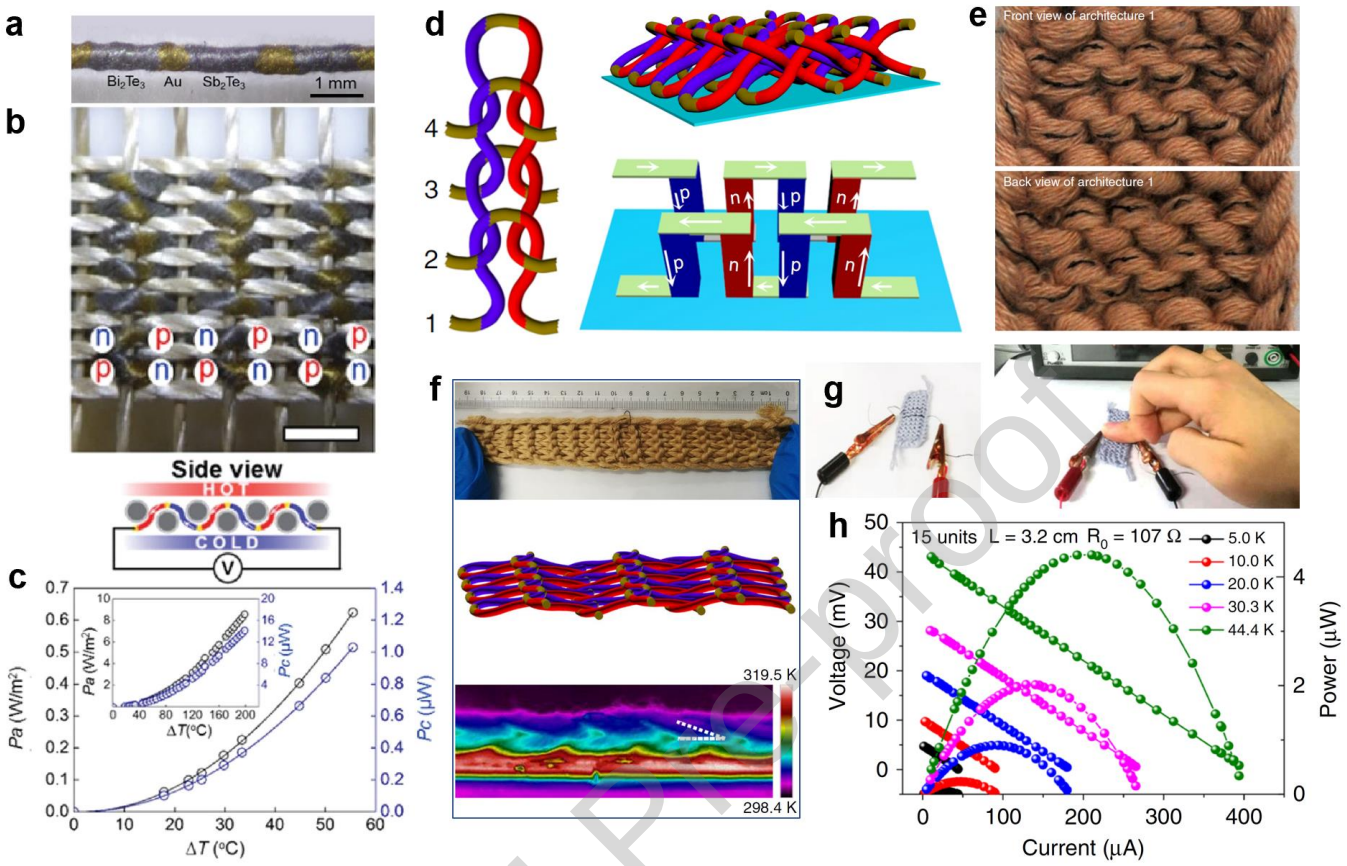

Figure 8. (a) Optical image of thermoelectric yarn with a (Au/Bi_2Te_3/Au/Sb_2Te_3)*n* structure. (b) Plain-weave thermoelectric textiles with an illustration of the side view. (c) Corresponding thermoelectric output. Reproduced with permission [90]. Copyright 2016 Wiley-VCH. (d) Schematic illustrations of thermoelectric textiles made by CNTs. (e) Optical images of the as-fabricated thermoelectric textiles. (f) Photographs of the top view and schematic and infrared thermal image of thermoelectric textile after longitudinal stretching by 80 %. (g) The methods for evaluating the thermoelectric output of thermoelectric textile. (h) The measured thermoelectric output of thermoelectric textile. Reproduced under a Creative Commons Attribution 4.0 International License [145]. Copyright 2020, Springer Nature.

Embroidery is also used to fabricate 3D fiber-based F-TEGs from thermoelectric yarns/filaments/fibers. For example, p-type nonionic waterborne polyurethane

(NWPU)/PEDOT:PSS/CNT-coated polyester yarns and n-type NWPU/N-doped CNT-coated polyester yarns can produce 2.6 nW power output at a temperature difference of 66 K [210]. In addition, a p-type CNT/PEG yarn was prepared by wet spinning and then coin it around a thin plastic strip, and then dropped n-type dopant on the surface of the plate. The formed product exhibited an output power of ~8 nW at a temperature difference of 25 K [133]. Besides, a similar method was applied to the p-type poly(3-hexylthiophene) (P3HT)-coated and n-type Ag paste-coated cotton threads, and the power output of 1.15 μW at a temperature difference of 50 K can be achieved [203].

4.2 Power generation

As shown in **Table 2**, the power supply of fiber-based F-TEGs is improving. The maximum power output of 1D fiber-based F-TEGs, made of p-type PEDOT:PSS/CNF and n-type polyethyleneimine (PEI)/CNT, has reached 6.25 μW at a temperature difference of 60 K [205]. The maximum output power of 460 nW at a ΔT of 30 K was observed in 2D fiber-based F-TEGs [93], but their flexibility remained a challenge. So far, the most appropriate 2D devices applied in the wearable electronics is the device made of p-type PEDOT:PSS and n-type Constantan with an output power of 212.6 nW [208]. However, the output power of 2D fiber-based F-TEGs may be changed due to their in-plane direction of the thermal gradient when integrating into the wearable electronics. 3D fiber-based F-TEGs are relatively rare compared with 1D/2D fiber-based F-TEGs because their device development is relevant new. However, it has been demonstrated that 3D devices have great potential to provide the most comfortable feeling due to their closely adherent to skins. The maximum power output of 14.1 μW at a ΔT of 200 K was demonstrated in 3D fiber-based FTEGs made of inorganic materials (p-type Sb_2Te_3 and n-type Bi_2Te_3) [90]. 3D fiber-based FTEGs made of hybrid materials (p-type NWPU/PEDOT:PSS/CNT and n-type NWPU/PEDOT:PSS/N-doped CNT) showed a maximum output power of 2.6 nW at the ΔT of 66 K

[197]. We anticipate that the demand for the development of 3D fiber-based F-TEGs will be needed for their scale-up production of wearable electronics in the future.

4.3 Refrigeration

Fiber-based F-TEGs can be also used for solid-state cooling with the opposite principle to the Seebeck effect, the Peltier cooling effect means that heat can be absorbed or released when an electric current is passed through the thermocouples. Peltier cooling has massive potential since the cooling process is not involved with the chemical reaction and mechanical moving, which is the most potential candidate that reduces the emission in the future. Normally, the Peltier cooling is widely used in electronics to provide the stable temperatures of the devices to avoid over-heat, but it requires a low thermal resistive environment and high heat load conditions to ensure its high efficiency in the ambient air [211]. Conventional methods to fabricate cooler to maintain their flexibility and low κ by using thermal co-evaporation, which has been used to deposit the inorganic materials on the organic composites. Besides, the thermal drawing technique is also developed to achieve both good wearability and high cooling performance [82]. To illustrate that thermoelectric fibers can be both used for power generation and refrigeration, Zhang *et al* assembled a thermoelectric rod through filling the powders of p-type $Bi_{0.5}Sb_{1.5}Te_3$ and n-type Bi_2Se_3 into a quartz tube, and then applied a vacuum oven to consolidate them [82]. After that, the thermoelectric fibers were fabricated through thermal drawing techniques to draw the thermoelectric rod in a vertical tube furnace at 1323 K, as illustrated in **Figure 9(a)** [82]. **Figure 9(b)** shows the optical photo of the as-fabricated core fibers [82], indicating good flexibility, and **Figure 9(c)** is the SEM image of an inorganic core fiber [82]. **Figure 9(d)** illustrates the method to evaluate the thermoelectric properties of the as-fabricated core fibers [82], and **Figure 9(e)** shows the measured thermoelectric power generation of F-TEG composed of p-type $Bi_{0.5}Sb_{1.5}Te_3$ fiber and n-type Bi_2Se_3 fiber, indicating a high output power of ~3 μW at a ΔT of 140 K [82]. In terms of the cooling

performance of the as-fabricated fibers, the fibers were woven into the fabric to form the flexible thermoelectric devices [82]. **Figure 9(f)** shows the simulated temperature profile of thermoelectric cooling with two pairs of p-n core fibers at an input current of 2 mA by finite element modelling [82], and **Figure 9(g)** shows corresponding experimental temperature profile recorded by infrared (IR) camera [82]. **Figure 9(h)** plots the evaluated thermoelectric cooling performance [82]. The results showed that thermoelectric devices can effectively achieve cooling of 5 degrees [82].

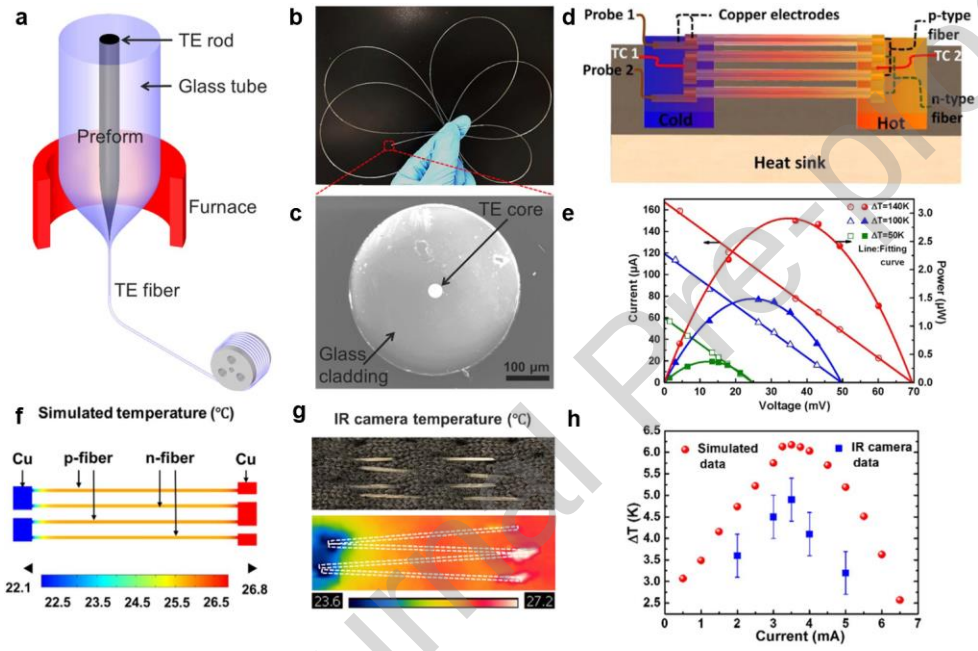

Figure 9. (a) Schematic diagram of the thermal drawing method to fabricate inorganic core fibers. (b) Optical photo and (c) SEM image of an inorganic core fiber. (d) Illustration of evaluating thermoelectric properties of as-fabricated core fibers. (e) Thermoelectric power generation of F-TEG composed of p-type $Bi_{0.5}Sb_{1.5}Te_3$ fiber and n-type Bi_2Se_3 fiber. (f) The simulated temperature profile of thermoelectric cooling with two pairs of p-n core fibers at an input current of 2 mA by finite element modelling. (g) Corresponding experimental temperature profile recorded by IR camera. (h) Evaluated thermoelectric cooling performance. Reproduced with permission [82]. Copyright 2017 Elsevier.

Conclusion, Challenges, and Outlook

Fiber-based thermoelectric materials and devices show great potentials for wearable electronics, and electronic-skin techniques. Current advances in fiber-based thermoelectric materials and devices have shown great potential to reduce the recharging times and save the life of batteries for most wearable electronics. Similar to the conventional materials, higher S and σ with lower κ is the development goal for better performance of fiber-based thermoelectric materials and devices. Fiber-based F-TEGs can be classified as three types of structures, which are the 1D structure (mainly the yarns/filament/ fibers), 2D structure (fabricated by coat the inorganic thermoelectric materials on the commercial fabric or fibers/yarns), and 3D structure (made of thermoelectric yarns/filaments/fibers). So far, 3D fiber-based F-TEGs show high-power output because they can easily adhere to the human skins, and intertwined yarns/filaments/fibers increase the area of harvesting energy. Inorganic thermoelectric alloys are appropriate materials for most TEGs due to their excellent thermoelectric properties while organic thermoelectric materials have perfect flexibility to adhere to human skins. There are also many kinds of studies integrating the inorganic and organic materials to generate hybrids with both high thermoelectric performance and high flexibility.

It should be noted that challenges are also significant for fiber-based materials and F-TEGs. Fabrication methods of 3D devices are more complicated compared with the methods to fabricating 1D and 2D devices since their needs for knitting, braiding, and weaving after thermoelectric materials being prepared. During the weaving, the p- and n-type elements need to be clearly distinguished, while wrong weaving, braiding, and knitting may lead to no voltage generated. Compared to the 3D structure, fabrications of the 2D structure are relatively simple, and most 2D F-TEGs can be fabricated by coating thermoelectric materials on conventional fabrics. However, these 2D F-TEGs always result in low comfortability and permeability. Moreover, although hybrids of inorganic and organic thermoelectric

materials have both relatively higher thermoelectric performance and flexibility, the thermoelectric performance of many hybrids is still lower than that of inorganic thermoelectric alloys, and the flexibility is lower than the pure organic polymers. Therefore, rational designs of both organic matrix and inorganic fillers are of significance [209]. For the outlook, **Figure 10** illustrates the potential directions for fiber-based thermoelectric materials and devices, and we anticipate that the following directions should pay more attention.

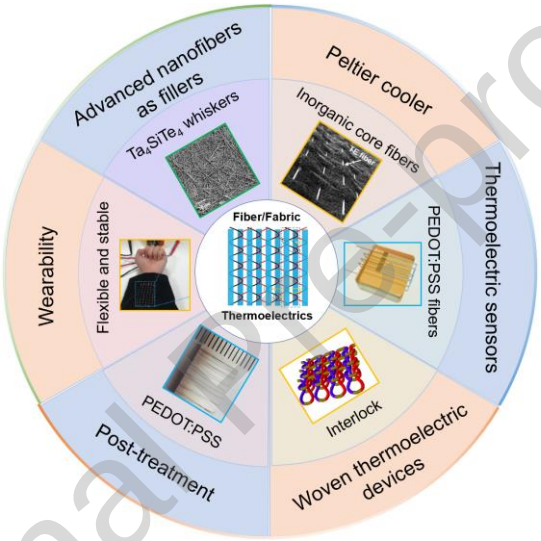

Figure 10. Strategies and outlooks for fiber-based thermoelectrics. In the center: fiber/fabric thermoelectrics. Reproduced with permission [78]. Copyright 2018 Wiley-VCH. Peltier cooler: Reproduced with permission [82]. Copyright 2017 Elsevier. Thermoelectric sensor: Reproduced under the Creative Commons Attribution License [177]. Copyright 2020 MDPI. Woven thermoelectric devices: Reproduced under a Creative Commons Attribution 4.0 International License [145]. Copyright 2020, Springer Nature. Post-treatment: Reproduced with permission [87]. Copyright 2020 Elsevier. Wearability: Reproduced with permission [84]. Copyright 2020 Wiley-VCH. Advanced nanofibers as fillers: Reproduced with permission [143]. Copyright 2020 Royal Society of Chemistry.

1. **Designing advanced nanofibers as fillers**. Compared with conventional fibers, nanofibers with dimensions close to quantum size (<100 nm) show great potential to have a similar or even higher *S* than the inorganic alloys due to the quantum confinement effect. Besides, nanofibers also possess higher flexibility than traditional fibers, therefore are more promising as fillers in organic/inorganic hybrid thermoelectric materials. The exploring of nanofibers with lower-dimensions can promise higher power output and solve the challenges of most of the inorganic material which is the low flexibility. However, attention should be paid to the protection of nanofibers since they are easily destroyed by oxidation or high temperatures. Therefore, the development of advanced fabrication techniques is required.

2. **Woven thermoelectric devices.** 3D fiber-based woven F-TEGs are one of the most potential candidates for charging wearable electronics since they can bring excellent breathability and flexibility. The weaving method still exits great potential to be explored since different weave structures can lead to a great difference in power output and flexibility, such as the interlock method [145]. The strategies of the new weaving methods and device structures are of significance to simplify the fabrication methods and improve the power output in 3D-structured fiber-based F-TEGs.

3. **Rational post-treatment.** The post-treatment can change the conformation and oxidation level of organic fiber-based thermoelectric materials and can lead to higher *ZT* values. However, the study of combining rational post-treatment into the fabrication of fiber-based F-TEGs has been rarely done. The appropriate post-treatment can further improve the thermoelectric performance during the fabrication of fiber-based F-TEGs, which can further improve the stability and flexibility. Therefore, the potential of the rational post-treatment in the fiber-based F-TEGs should be explored.

4. **Development of Peltier cooler and relevant sensors**. High-performance Peltier coolers are important functional devices due to its considerable advantages, such as silent working, no moving parts, small size, and invulnerability to leaks. However, only very few fiber-based Peltier coolers have been

developed [82], suggesting that this research area, including fabrication methods and device development strategies, needs further exploration with a focus on achieving higher cooling efficiency.

5. **Wearability improvement**. The wearability is critical for the development of fiber-based thermoelectric materials and devices in the future. However, most current studies mainly focused on the thermoelectric performance of materials and devices. Therefore, the research on the high wearability for the F-TEGs should be in progress simultaneously.

Overall, this review comprehensively summarizes the fundamentals, progress, challenge, and perspective of fiber-based thermoelectric materials and devices. We hope this review can provide guidance to the future development of fiber-based thermoelectrics.

Acknowlegement

This work is financially supported by the Australian Research Council, Innovation Centre for Sustainable Steel Project, and USQ strategic research grant.

References

[1] X.-L. Shi, J. Zou, and Z.-G. Chen, Chem. Rev. 120 (2020) 7399-7515.

[2] L. Huang, S. Lin, Z. Xu, H. Zhou, J. Duan, B. Hu, and J. Zhou, Adv. Mater. 32 (2020) 1902034.

[3] Y. Wang, L. Yang, X. Shi, X. Shi, L. Chen, M. Dargusch, J. Zou, and Z.-G. Chen, Adv. Mater. 31 (2019) 1807916.

[4] K. Kanahashi, J. Pu, and T. Takenobu, Adv. Energy Mater. 10 (2020) 1902842.

[5] X. Shi and L. Chen, Nat. Mater. 15 (2016) 691-692.

[6] Y. Xiao and L.-D. Zhao, Science 367 (2020) 1196.

[7] B. Cai, H. Hu, H.-L. Zhuang, and J.-F. Li, J. Alloys Compd. 806 (2019) 471-486.

[8] Y. Du, J. Xu, B. Paul, and P. Eklund, Appl. Mater. Today 12 (2018) 366-388.

[9] Y. Pei, X. Shi, A. LaLonde, H. Wang, L. Chen, and G.J. Snyder, Nature 473 (2011) 66-69.

[10] Y. Pei, A. LaLonde, S. Iwanaga, and G.J. Snyder, Energy Environ. Sci. 4 (2011) 2085-2089.

[11] A. Suwardi, J. Cao, Y. Zhao, J. Wu, S.W. Chien, X.Y. Tan, L. Hu, X. Wang, W. Wang, D. Li, Y. Yin, W.-X. Zhou, D.V.M. Repaka, J. Chen, Y. Zheng, Q. Yan, G. Zhang, and J. Xu, Mater. Today Phys. (2020) 100239.

[12] T. Fu, X. Yue, H. Wu, C. Fu, T. Zhu, X. Liu, L. Hu, P. Ying, J. He, and X. Zhao, J. Materiomics 2 (2016) 141-149.

[13] K. Ahn, K. Biswas, J. He, I. Chung, V. Dravid, and M.G. Kanatzidis, Energy Environ. Sci. 6 (2013) 1529-1537.

[14] Y. Pei, A.D. LaLonde, N.A. Heinz, and G.J. Snyder, Adv. Energy Mater. 2 (2012) 670-675.

[15] B. Xiang, J. Liu, J. Yan, M. Xia, Q. Zhang, L. Chen, J. Li, X.Y. Tan, Q. Yan, and Y. Wu, J. Mater. Chem. A 7 (2019) 18458-18467.

[16] Y. Pei, Z.M. Gibbs, A. Gloskovskii, B. Balke, W.G. Zeier, and G.J. Snyder, Adv. Energy Mater. 4 (2014) 1400486.

[17] W. Liu, X. Shi, R. Moshwan, M. Hong, L. Yang, Z.-G. Chen, and J. Zou, Sustain. Mater. Technol. 17 (2018) e00076.

[18] W.-D. Liu, L. Yang, and Z.-G. Chen, Nano Today 35 (2020) 100938.

[19] W. Liu, L. Yang, Z.-G. Chen, and J. Zou, Adv. Mater. 32 (2020) 1905703.

[20] K. Zhao, P. Qiu, X. Shi, and L. Chen, Adv. Funct. Mater. 30 (2019) 1903867.

[21] W. Liu, X. Shi, M. Hong, L. Yang, R. Moshwan, Z.-G. Chen, and J. Zou, J. Mater. Chem. C 6 (2018) 13225-13231.

[22] K. Qian, L. Gao, X. Chen, H. Li, S. Zhang, X.-L. Zhang, S. Zhu, J. Yan, D. Bao, L. Cao, J.-A. Shi, J. Lu, C. Liu, J. Wang, T. Qian, H. Ding, L. Gu, W. Zhou, Y.-Y. Zhang, X. Lin, S. Du, M. Ouyang, S.T. Pantelides, and H.-J. Gao, Adv. Mater. 32 (2020) 1908314.

[23] D. Yang, X. Su, J. Li, H. Bai, S. Wang, Z. Li, H. Tang, K. Tang, T. Luo, Y. Yan, J. Wu, J. Yang, Q. Zhang, C. Uher, M.G. Kanatzidis, and X. Tang, Adv. Mater. 32 (2020) 2003730.

[24] T. Mao, P. Qiu, X. Du, P. Hu, K. Zhao, J. Xiao, X. Shi, and L. Chen, Adv. Funct. Mater. 30 (2020) 1908315.

[25] P. Lu, H. Liu, X. Yuan, F. Xu, X. Shi, K. Zhao, W. Qiu, W. Zhang, and L. Chen, J. Mater. Chem. A 3 (2015) 6901-6908.

[26] M. Li, D.L. Cortie, J. Liu, D. Yu, S.M.K.N. Islam, L. Zhao, D.R. Mitchell, R.A. Mole, M.B. Cortie, and S. Dou, Nano Energy 53 (2018) 993-1002.

[27] W.-D. Liu, X.-L. Shi, R. Moshwan, L. Yang, Z.-G. Chen, and J. Zou, Chem. Eng. J. 375 (2019) 121996.

[28] M. Hong, K. Zheng, W. Lyv, M. Li, X. Qu, Q. Sun, S. Xu, J. Zou, and Z.-G. Chen, Energy Environ. Sci. 13 (2020) 1856-1864.

[29] X. Zhang, Z. Bu, S. Lin, Z. Chen, W. Li, and Y. Pei, Joule 4 (2020) 986-1003.

[30] W.-D. Liu, D.-Z. Wang, Q. Liu, W. Zhou, Z. Shao, and Z.-G. Chen, Adv. Energy Mater. 10 (2020) 2000367.

[31] L. Xie, Y. Chen, R. Liu, E. Song, T. Xing, T. Deng, Q. Song, J. Liu, R. Zheng, X. Gao, S. Bai, and L. Chen, Nano Energy 68 (2020) 104347.

[32] E. Nshimyimana, S. Hao, X. Su, C. Zhang, W. Liu, Y. Yan, C. Uher, C. Wolverton, M.G. Kanatzidis, and X. Tang, J. Mater. Chem. A 8 (2020) 1193-1204.

[33] K.s. Bayikadi, S. Raman, C.T. Wu, L.-C. Chen, K.H. Chen, and F.-C. Chou, J. Mater. Chem. A 8 (2020) 5332-5341.

[34] L. Wang, J. Li, C. Zhang, T. Ding, Y. Xie, Y. Li, F. Liu, W. Ao, and C. Zhang, J. Mater. Chem. A 8 (2020) 1660-1667.

[35] G. Xie, Z. Li, T. Luo, H. Bai, J. Sun, Y. Xiao, L.-D. Zhao, J. Wu, G. Tan, and X. Tang, Nano Energy 69 (2020) 104395.

[36] J. Shuai, Y. Sun, X. Tan, and T. Mori, Small 16 (2020) 1906921.

[37] P. Li, T. Ding, J. Li, C. Zhang, Y. Dou, Y. Li, L. Hu, F. Liu, and C. Zhang, Adv. Funct. Mater. 30 (2020) 1910059.

[38] M. Li, M. Hong, X. Tang, Q. Sun, W.-Y. Lyu, S.-D. Xu, L.-Z. Kou, M. Dargusch, J. Zou, and Z.-G. Chen, Nano Energy 73 (2020) 104740.

[39] J. Dong, F.-H. Sun, H. Tang, J. Pei, H.-L. Zhuang, H.-H. Hu, B.-P. Zhang, Y. Pan, and J.-F. Li, Energy Environ. Sci. 12 (2019) 1396-1403.

[40] X. Shi, Z.-G. Chen, W. Liu, L. Yang, M. Hong, R. Moshwan, L. Huang, and J. Zou, Energy Storage Mater. 10 (2018) 130-138.

[41] L. Huang, J. Lu, D. Ma, C. Ma, B. Zhang, H. Wang, G. Wang, D. Gregory, X. Zhou, and G. Han, J. Mater. Chem. A 8 (2020) 1394-1402.

[42] X.L. Shi, K. Zheng, M. Hong, W.D. Liu, R. Moshwan, Y. Wang, X.-L. Qu, Z.G. Chen, and J. Zou, Chem. Sci. 9 (2018) 7376-7389.

[43] L.D. Zhao, S.H. Lo, Y. Zhang, H. Sun, G. Tan, C. Uher, C. Wolverton, V.P. Dravid, and M.G. Kanatzidis, Nature 508 (2014) 373-377.

[44] X. Shi, A. Wu, T. Feng, K. Zheng, W. Liu, Q. Sun, M. Hong, S.T. Pantelides, Z.G. Chen, and J. Zou, Adv. Energy Mater. 9 (2019) 1803242.

[45] K. Peng, X. Lu, H. Zhan, S. Hui, X. Tang, G. Wang, J. Dai, C. Uher, G. Wang, and X. Zhou, Energy Environ. Sci. 9 (2016) 454-460.

[46] X. Shi, A. Wu, W. Liu, R. Moshwan, Y. Wang, Z.-G. Chen, and J. Zou, ACS Nano 12 (2018) 11417-11425.

[47] L. Mao, Y. Yin, Q. Zhang, G.-Q. Liu, H. Wang, Z. Guo, H. Hu, Y. Xiao, X. Tan, and J. Jiang, Energy Environ. Sci. 13 (2020) 616-621.

[48] X.L. Shi, K. Zheng, W.D. Liu, Y. Wang, Y.Z. Yang, Z.G. Chen, and J. Zou, Adv. Energy Mater. 8 (2018) 1800775.

[49] Y.-X. Chen, X.-L. Shi, Z.-H. Zheng, F. Li, W.-D. Liu, W.-Y. Chen, X.-R. Li, G.-X. Liang, J.-T. Luo, P. Fan, and Z.-G. Chen, Mater. Today Phys. 16 (2020) 100306.

[50] Y. Zheng, X.-L. Shi, H. Yuan, S. Lu, X. Qu, W. Liu, L. Wang, K. Zheng, J. Zou, and Z.-G. Chen, Mater. Today Phys. 13 (2020) 100198.

[51] X.-L. Shi, X. Tao, J. Zou, and Z.-G. Chen, Adv. Sci. 7 (2020) 1902923.

[52] M. Dargusch, X.-L. Shi, X.Q. Tran, T. Feng, F. Somidin, X. Tan, W. Liu, K. Jack, J. Venezuela, H. Maeno, T. Toriyama, S. Matsumura, S.T. Pantelides, and Z.-G. Chen, J. Phys. Chem. Lett. 10 (2019) 6512-6517.

[53] X.-L. Shi, W.-D. Liu, A.-Y. Wu, V.T. Nguyen, H. Gao, Q. Sun, R. Moshwan, J. Zou, and Z.-G. Chen, InfoMat 2 (2020) 1201-1215.

[54] M. Jin, X.-L. Shi, T. Feng, W. Liu, H. Feng, S.T. Pantelides, J. Jiang, Y. Chen, Y. Du, J. Zou, and Z.-G. Chen, ACS Appl. Mater. Interfaces 11 (2019) 8051-8059.

[55] R. Moshwan, X.-L. Shi, W.-D. Liu, L. Yang, Y. Wang, M. Hong, G. Auchterlonie, J. Zou, and Z.-G. Chen, ACS Appl. Mater. Interfaces 10 (2018) 38944-38952.

[56] R. Moshwan, L. Yang, J. Zou, and Z.-G. Chen, Adv. Funct. Mater. 27 (2017) 1703278.

[57] R. Moshwan, W.-D. Liu, X.-L. Shi, Y.-P. Wang, J. Zou, and Z.-G. Chen, Nano Energy 65 (2019) 104056.

[58] R. Moshwan, W.-D. Liu, X.-L. Shi, Q. Sun, H. Gao, Y.-P. Wang, J. Zou, and Z.-G. Chen, J. Mater. Chem. A 8 (2020) 3978-3987.

[59] Q. Zhang, Z. Guo, X. Tan, L. Mao, Y. Yin, Y. Xiao, H. Hu, C. Tan, Q. Wu, G.-Q. Liu, J. Xu, and J. Jiang, Chem. Eng. J. 390 (2020) 124585.

[60] D. Sarkar, T. Ghosh, A. Banik, S. Roychowdhury, D. Sanyal, and K. Biswas, Angew. Chem. Int. Ed. 59 (2020) 2-10.

[61] S. Li, J. Xin, A. Basit, Q. Long, S. Li, Q. Jiang, Y. Luo, and J. Yang, Adv. Sci. (2020) 1903493.

[62] H. Ju and J. Kim, Chem. Eng. J. 402 (2020) 126274.

[63] R. Moshwan, X.-L. Shi, W.-D. Liu, Y. Wang, S. Xu, J. Zou, and Z.-G. Chen, ACS Appl. Energy Mater. 2 (2019) 2965-2971.

[64] M. Hong, Z.-G. Chen, and J. Zou, Chinese Phys. B 27 (2018) 048403.

[65] Y. Wang, W.-D. Liu, X.-L. Shi, M. Hong, L.-J. Wang, M. Li, H. Wang, J. Zou, and Z.-G. Chen, Chem. Eng. J. 391 (2019) 123513.

[66] D. Bao, J. Chen, Y. Yu, W. Liu, L. Huang, G. Han, J. Tang, D. Zhou, L. Yang, and Z.-G. Chen, Chem. Eng. J. 388 (2020) 124295.

[67] H. Shang, C. Dun, Y. Deng, T. Li, Z. Gao, L. Xiao, H. Gu, D.J. Singh, Z. Ren, and F. Ding, J. Mater. Chem. A 8 (2020) 4552-4561.

[68] Y. Zhou, F. Meng, J. He, A. Benton, L. Hu, F. Liu, J. Li, C. Zhang, W. Ao, and H. Xie, ACS Appl. Mater. Interfaces 12 (2020) 31619-31627.

[69] L. Hu, F. Meng, Y. Zhou, J. Li, A. Benton, J. Li, F. Liu, C. Zhang, H. Xie, and J. He, Adv. Funct. Mater. 30 (2020) 2005202.

[70] Y. Wang, W. Liu, H. Gao, L. Wang, M. Li, X.-L. Shi, M. Hong, H. Wang, J. Zou, and Z.-G. Chen, ACS Appl. Mater. Interfaces 11 (2019) 31237-31244.

[71] M. Tan, W.-D. Liu, X.-L. Shi, J. Shang, H. Li, X. Liu, L. Kou, M. Dargusch, Y. Deng, and Z.-G. Chen, Nano Energy 78 (2020) 105379.

[72] X.-L. Shi, W.-Y. Chen, X. Tao, J. Zou, and Z.-G. Chen, Mater. Horiz. (2020). DOI: 10.1039/D0MH00954G.

[73] Y. Wang, M. Hong, W.-D. Liu, X.-L. Shi, S.-D. Xu, Q. Sun, H. Gao, S. Lu, J. Zou, and Z.-G. Chen, Chem. Eng. J. 397 (2020) 125360.

[74] M. Tan, W.D. Liu, X.L. Shi, H. Gao, H. Li, C. Li, X.B. Liu, Y. Deng, and Z.G. Chen, Small Methods 3 (2019) 1900582.

[75] B. Cai, H.-L. Zhuang, Q. Cao, H. Hu, J. Dong, Asfandiyar, and J.-F. Li, ACS Appl. Mater. Interfaces 12 (2020) 16426-16435.

[76] Y. Zhang and S.-J. Park, Polymers 11 (2019) 909.

[77] M. Bharti, A. Singh, S. Samanta, and D.K. Aswal, Prog. Mater. Sci. 93 (2018) 270-310.

[78] L. Zhang, S. Lin, T. Hua, B. Huang, S. Liu, and X. Tao, Adv. Energy Mater. 8 (2018) 1700524.

[79] C.S. Kim, H.M. Yang, J. Lee, G.S. Lee, H. Choi, Y.J. Kim, S.H. Lim, S.H. Cho, and B.J. Cho, ACS Energy Lett. 3 (2018) 501-507.

[80] E.J.X. Pang, S.J. Pickering, A. Chan, K.H. Wong, and P.L. Lau, J. Solid State Chem. 193 (2012) 147-153.

[81] F. Ren, P. Menchhofer, J. Kiggans, and H. Wang, J. Electron. Mater. 45 (2016) 1412-1418.

[82] T. Zhang, K. Li, J. Zhang, M. Chen, Z. Wang, S. Ma, N. Zhang, and L. Wei, Nano Energy 41 (2017) 35-42.

[83] M. Sun, Q. Qian, G. Tang, W. Liu, G. Qian, Z. Shi, K. Huang, D. Chen, S. Xu, and Z. Yang, APL Mater. 6 (2018) 036103.

[84] J. Zhang, T. Zhang, H. Zhang, Z. Wang, C. Li, Z. Wang, K. Li, X. Huang, M. Chen, Z. Chen, Z. Tian, H. Chen, L.-D. Zhao, and L. Wei, Adv. Mater. 32 (2020) 2002702.

[85] B. Endrődi, J. Mellár, Z. Gingl, C. Visy, and C. Janáky, RSC Adv. 4 (2014) 55328-55333.

[86] S. Hiura, N. Okada, J. Wakui, H. Narita, S. Kanehashi, and T. Shimomura, Materials 10 (2017) 468.

[87] N. Wen, Z. Fan, S. Yang, Y. Zhao, T. Cong, S. Xu, H. Zhang, J. Wang, H. Huang, C. Li, and L. Pan, Nano Energy 78 (2020) 105361.

[88] S. Han and D.D.L. Chung, Compos. Part A-appl. S. 48 (2013) 162-170.

[89] S.J. Kim, J.H. We, and B.J. Cho, Energy Environ. Sci. 7 (2014) 1959-1965.

[90] J.A. Lee, A.E. Aliev, J.S. Bykova, M.J. de Andrade, D. Kim, H.J. Sim, X. Lepró, A.A. Zakhidov, J.-B. Lee, G.M. Spinks, S. Roth, S.J. Kim, and R.H. Baughman, Adv. Mater. 28 (2016) 5038-5044.

[91] S. Shin, R. Kumar, J.W. Roh, D.-S. Ko, H.-S. Kim, S.I. Kim, L. Yin, S.M. Schlossberg, S. Cui, J.-M. You, S. Kwon, J. Zheng, J. Wang, and R. Chen, Sci. Rep. 7 (2017) 7317.

[92] Q. Jin, W. Shi, Y. Zhao, J. Qiao, J. Qiu, C. Sun, H. Lei, K. Tai, and X. Jiang, ACS Appl. Mater. Interfaces 10 (2018) 1743-1751.

[93] Y. Ding, Y. Qiu, K. Cai, Q. Yao, S. Chen, L. Chen, and J. He, Nat. Commun. 10 (2019) 841.

[94] G. Tan, L.D. Zhao, and M.G. Kanatzidis, Chem. Rev. 116 (2016) 12123-12149.

[95] L. Yang, Z.-G. Chen, M.S. Dargusch, and J. Zou, Adv. Energy Mater. 8 (2017) 1701797.

[96] J.R. Sootsman, D.Y. Chung, and M.G. Kanatzidis, Angew. Chem. Int. Ed. 48 (2009) 8616-8639.

[97] D. Li, Y. Gong, Y. Chen, J. Lin, Q. Khan, Y. Zhang, Y. Li, H. Zhang, and H. Xie, Nano-Micro Lett. 12 (2020) 36.

[98] J. Wei, L. Yang, Z. Ma, P. Song, M. Zhang, J. Ma, F. Yang, and X. Wang, J. Mater. Sci. 55 (2020) 12642-12704.

[99] Y. Zeng and A. Marconnet, Rev. Sci. Instrum. 88 (2017) 044901.

[100] S. Hooshmand Zaferani, R. Ghomashchi, and D. Vashaee, Renew. Sust. Energ. Rev. 112 (2019) 158-169.

[101] G.J. Snyder and E.S. Toberer, Nat. Mater. 7 (2008) 105-114.

[102] G. Kim, L. Shao, K. Zhang, and K.P. Pipe, Nat. Mater. 12 (2013) 719-723.

[103] İ. İlhan and A.Y. Yarar, J. Text. I. 107 (2016) 1185-1192.

[104] Y.E. Mogahzy and C. Charles, Auburn. edu (1993). Retrieved from http://www.tex.tuiasi.ro/biblioteca/carti/Articole.

[105] K. Klemola, J. Pearson, J. Liesivuori, and P. Lindström-Seppä, J. Text. I. 100 (2009) 330-337.

[106] A. Birhanlı and M. Ozmen, Drug Chem. Toxicol. 28 (2005) 51-65.

[107] T. Estlander, Contact. Dermatitis 18 (1988) 290-297.

[108] B. García Bracamonte, F.J. Ortiz de Frutos, and L. Iglesias Díez, Contact. Dermatitis 33 (1995) 139-140.

[109] C.A. Gonzales, E. Riboli, and G. Lopez-Abente, Am. J. Ind. Med. 14 (1988) 673-680.

[110] K.L. Hatch and H.I. Maibach, J. Am. Acad. Dermatol. 32 (1995) 631-639.

[111] N. Mathur, P. Bhatnagar, P. Nagar, and M.K. Bijarnia, Ecotox. Environ. Safe. 61 (2005) 105-113.

[112] L. Corchia, G. Monti, and L. Tarricone, Int. J. Antenn. Propag. 2018 (2018) 2340293.

[113] D.R. Seshadri, C. Drummond, J. Craker, J.R. Rowbottom, and J.E. Voos, IEEE Pulse 8 (2017) 38-43.

[114] E.J.X. Pang, A. Chan, and S.J. Pickering, Compos. Part A-appl. S. 42 (2011) 1406-1411.

[115] D. Liang, H. Yang, S.W. Finefrock, and Y. Wu, Nano Lett. 12 (2012) 2140-2145.

[116] M. Zhang, H. Park, J. Kim, H. Park, T. Wu, S. Kim, S.-D. Park, Y. Choa, and N.V. Myung, Chem. Mater. 27 (2015) 5189-5197.

[117] W. Ma, Y. Liu, S. Yan, T. Miao, S. Shi, M. Yang, X. Zhang, and C. Gao, Nano Res. 9 (2016) 3536-3546.

[118] L. Tzounis, C. Gravalidis, S. Vassiliadou, and S. Logothetidis, Mater. Today P. 4 (2017) 7070-7075.

[119] W. Ma, Y. Liu, S. Yan, T. Miao, S. Shi, Z. Xu, X. Zhang, and C. Gao, Nano Res. 11 (2018) 741-750.

[120] P.R. Jagadish, M. Khalid, L.P. Li, M.T. Hajibeigy, N. Amin, R. Walvekar, and A. Chan, J. Clean. Prod. 195 (2018) 1015-1025.

[121] G. Qian, M. Sun, G. Tang, W. Liu, Z. Shi, Q. Qian, Q. Zhang, and Z. Yang, Mater. Lett. 233 (2018) 63-66.

[122] A. Morata, M. Pacios, G. Gadea, C. Flox, D. Cadavid, A. Cabot, and A. Tarancón, Nat. Commun. 9 (2018) 4759.

[123] P. Jagadish, M. Khalid, N. Amin, M.T. Hajibeigy, L.P. Li, A. Numan, N.M. Mubarak, R. Walvekar, and A. Chan, Compos. Part B-eng. 175 (2019) 107085.

[124] Q. Yao, L. Chen, X. Xu, and C. Wang, Chem. Lett. 34 (2005) 522-523.

[125] J. Wu, Y. Sun, W.-B. Pei, L. Huang, W. Xu, and Q. Zhang, Synthetic. Met. 196 (2014) 173-177.

[126] X. Hu, G. Chen, X. Wang, and H. Wang, J. Mater. Chem. A 3 (2015) 20896-20902.

[127] J. Liu, Y. Jia, Q. Jiang, F. Jiang, C. Li, X. Wang, P. Liu, P. Liu, F. Hu, Y. Du, and J. Xu, ACS Appl. Mater. Interfaces 10 (2018) 44033-44040.

[128] Q. Wang, Q. Yao, J. Chang, and L. Chen, J. Mater. Chem. 22 (2012) 17612-17618.

[129] Q. Jiang, C. Liu, J. Xu, B. Lu, H. Song, H. Shi, Y. Yao, and L. Zhang, J. Polym. Sci. Pol. Phys. 52 (2014) 737-742.

[130] D. Wang, Y. Su, D. Chen, L. Wang, X. Xiang, and D. Zhu, Compos. Part B-eng. 69 (2015) 467-471.

[131] M. Piao, M.-K. Joo, J.H. Choi, J.M. Shin, Y.S. Moon, G.T. Kim, and U. Dettlaff-Weglikowska, RSC Adv. 5 (2015) 78099-78103.

[132] Y. Du, K. Cai, S. Chen, H. Wang, S.Z. Shen, R. Donelson, and T. Lin, Sci. Rep. 5 (2015) 6411.

[133] M. Ito, T. Koizumi, H. Kojima, T. Saito, and M. Nakamura, J. Mater. Chem. A 5 (2017) 12068-12072.

[134] Y. Du, J. Xu, Y. Wang, and T. Lin, J. Mater. Sci. Mater. El. 28 (2017) 5796-5801.

[135] K. Kirihara, Q. Wei, M. Mukaida, and T. Ishida, Synthetic. Met. 225 (2017) 41-48.

[136] J.-Y. Kim, W. Lee, Y.H. Kang, S.Y. Cho, and K.-S. Jang, Carbon 133 (2018) 293-299.

[137] S. Xin, N. Yang, F. Gao, J. Zhao, L. Li, and C. Teng, Mater. Chem. Phys. 212 (2018) 440-445.

[138] X. Chen, G. Tang, J. Pan, and H. Wang, J. Miner. Mater. Char. Eng. 6 (2018) 448-463.

[139] G. Karalis, L. Tzounis, E. Lambrou, L.N. Gergidis, and A.S. Paipetis, Appl. Energ. 253 (2019) 113512.

[140] N. Dalton, R.P. Lynch, M.N. Collins, and M. Culebras, Int. J. Biol. Macromol. 121 (2019) 472-479.

[141] X. Lan, T. Wang, C. Liu, P. Liu, J. Xu, X. Liu, Y. Du, and F. Jiang, Compos. Sci. Technol. 182 (2019) 107767.

[142] Y. Zheng, Q. Zhang, W. Jin, Y. Jing, X. Chen, X. Han, Q. Bao, Y. Liu, X. Wang, S. Wang, Y. Qiu, C.-a. Di, and K. Zhang, J. Mater. Chem. A 8 (2020) 2984-2994.

[143] Q. Xu, S. Qu, C. Ming, P. Qiu, q. yao, C. Zhu, T.-R. Wei, J. He, X. Shi, and L. Chen, Energy Environ. Sci. 13 (2020) 511-518.

[144] H. Xu, Y. Guo, B. Wu, C. Hou, Q. Zhang, Y. Li, and H. Wang, ACS Appl. Mater. Interfaces 12 (2020) 33297-33304.

[145] T. Sun, B. Zhou, Q. Zheng, L. Wang, W. Jiang, and G.J. Snyder, Nat. Commun. 11 (2020) 572.

[146] T. Dongyan, L. Hong, and C. Weimin, Ferroelectrics 265 (2002) 259-264.

[147] H. Khayyam, R.N. Jazar, S. Nunna, G. Golkarnarenji, K. Badii, S.M. Fakhrhoseini, S. Kumar, and M. Naebe, Prog. Mater. Sci. 107 (2020) 100575.

[148] L. Wang and K. Zhang, Energy Environ. Mater. 3 (2020) 67-79.

[149] X.-L. Shi, H. Wu, Q. Liu, W. Zhou, S. Lu, Z. Shao, M. Dargusch, and Z.-G. Chen, Nano Energy 78 (2020) 105195.

[150] Y. Lin, J. Liu, X. Wang, J. Xu, P. Liu, G. Nie, C. Liu, and F. Jiang, Compos. Commun. 16 (2019) 79-83.

[151] T. Lee, K.T. Park, B.-C. Ku, and H. Kim, Nanoscale 11 (2019) 16919-16927.

[152] A.D. Avery, B.H. Zhou, J. Lee, E.-S. Lee, E.M. Miller, R. Ihly, D. Wesenberg, K.S. Mistry, S.L. Guillot, B.L. Zink, Y.-H. Kim, J.L. Blackburn, and A.J. Ferguson, Nat. Energy 1 (2016) 16033.

[153] T. Miao, W. Ma, X. Zhang, J. Wei, and J. Sun, Appl. Phys. Lett. 102 (2013) 053105.

[154] L. Shi, D. Li, C. Yu, W. Jang, D. Kim, Z. Yao, P. Kim, and A. Majumdar, J. Heat Trans. 125 (2003) 881-888.

[155] J. Hone, M.C. Llaguno, N.M. Nemes, A.T. Johnson, J.E. Fischer, D.A. Walters, M.J. Casavant, J. Schmidt, and R.E. Smalley, Appl. Phys. Lett. 77 (2000) 666-668.

[156] R. Jin, Z.X. Zhou, D. Mandrus, I.N. Ivanov, G. Eres, J.Y. Howe, A.A. Puretzky, and D.B. Geohegan, Physica. B 388 (2007) 326-330.

[157] H.-L. Zhang, J.-F. Li, B.-P. Zhang, K.-F. Yao, W.-S. Liu, and H. Wang, Phys. Rev. B 75 (2007) 205407.

[158] C.A. Hewitt, A.B. Kaiser, M. Craps, R. Czerw, and D.L. Carroll, J. Appl. Phys. 114 (2013) 083701.

[159] Y. Nonoguchi, K. Ohashi, R. Kanazawa, K. Ashiba, K. Hata, T. Nakagawa, C. Adachi, T. Tanase, and T. Kawai, Sci. Rep. 3 (2013) 3344.

[160] C.A. Hewitt, M. Craps, R. Czerw, and D.L. Carroll, Synthetic. Met. 184 (2013) 68-72.

[161] S.L. Kim, K. Choi, A. Tazebay, and C. Yu, ACS Nano 8 (2014) 2377-2386.

[162] Y. Nakai, K. Honda, K. Yanagi, H. Kataura, T. Kato, T. Yamamoto, and Y. Maniwa, Appl. Phys. Express 7 (2014) 025103.

[163] M. Piao, M.-K. Joo, J. Na, Y.-J. Kim, M. Mouis, G. Ghibaudo, S. Roth, W.-Y. Kim, H.-K. Jang, G.P. Kennedy, U. Dettlaff-Weglikowska, and G.-T. Kim, J. Phys. Chem. C 118 (2014) 26454-26461.

[164] L. Zhao, X. Sun, Z. Lei, J. Zhao, J. Wu, Q. Li, and A. Zhang, Compos. Part B-eng. 83 (2015) 317-322.

[165] D. Hayashi, T. Ueda, Y. Nakai, H. Kyakuno, Y. Miyata, T. Yamamoto, T. Saito, K. Hata, and Y. Maniwa, Appl. Phys. Express 9 (2016) 025102.

[166] T. Miao, S. Shi, S. Yan, W. Ma, X. Zhang, K. Takahashi, and T. Ikuta, J. Appl. Phys. 120 (2016) 124302.

[167] G. Wu, C. Gao, G. Chen, X. Wang, and H. Wang, J. Mater. Chem. A 4 (2016) 14187-14193.

[168] J.H. Seol, I. Jo, A.L. Moore, L. Lindsay, Z.H. Aitken, M.T. Pettes, X. Li, Z. Yao, R. Huang, D. Broido, N. Mingo, R.S. Ruoff, and L. Shi, Science 328 (2010) 213.

[169] N. Xiao, X. Dong, L. Song, D. Liu, Y. Tay, S. Wu, L.-J. Li, Y. Zhao, T. Yu, H. Zhang, W. Huang, H.H. Hng, P.M. Ajayan, and Q. Yan, ACS Nano 5 (2011) 2749-2755.

[170] D. Sim, D. Liu, X. Dong, N. Xiao, S. Li, Y. Zhao, L.-J. Li, Q. Yan, and H.H. Hng, J. Phys. Chem. C 115 (2011) 1780-1785.

[171] Z. Wang, R. Xie, C.T. Bui, D. Liu, X. Ni, B. Li, and J.T.L. Thong, Nano Lett. 11 (2011) 113-118.

[172] A.V. Babichev, V.E. Gasumyants, and V.Y. Butko, J. Appl. Phys. 113 (2013) 076101.

[173] Y. Guo, J. Mu, C. Hou, H. Wang, Q. Zhang, and Y. Li, Carbon 107 (2016) 146-153.

[174] J.L. Blackburn, A.J. Ferguson, C. Cho, and J.C. Grunlan, Adv. Mater. 30 (2018) 1704386.

[175] W. Zhao, S. Fan, N. Xiao, D. Liu, Y.Y. Tay, C. Yu, D. Sim, H.H. Hng, Q. Zhang, and F. Boey, Energy Environ. Sci. 5 (2012) 5364-5369.

[176] W. Liu, J. Zhang, and H. Liu, Polymers 11 (2019) 954.

[177] L. Ruan, Y. Zhao, Z. Chen, W. Zeng, S. Wang, D. Liang, and J. Zhao, Polymers 12 (2020) 553.

[178] Y. Kim, T. Lim, C.-H. Kim, C.S. Yeo, K. Seo, S.-M. Kim, J. Kim, S.Y. Park, S. Ju, and M.-H. Yoon, NPG Asia Mater. 10 (2018) 1086-1095.

[179] S. Xu, M. Hong, X.-L. Shi, M. Li, Q. Sun, Q. Chen, M. Dargusch, J. Zou, and Z.-G. Chen, Energy Environ. Sci. 13 (2020) 3480-3488.

[180] S. Xu, M. Hong, X.-L. Shi, Y. Wang, L. Ge, Y. Bai, L. Wang, M. Dargusch, J. Zou, and Z.-G. Chen, Chem. Mater. 31 (2019) 5238-5244.

[181] S. Liu, H. Deng, Y. Zhao, S. Ren, and Q. Fu, RSC Adv. 5 (2015) 1910-1917.

[182] W. Shi, Z. Shuai, and D. Wang, Adv. Funct. Mater. 27 (2017) 1702847.

[183] K. Sun, S. Zhang, P. Li, Y. Xia, X. Zhang, D. Du, F.H. Isikgor, and J. Ouyang, J. Mater. Sci. Mater. El. 26 (2015) 4438-4462.

[184] K.-C. Chang, M.-S. Jeng, C.-C. Yang, Y.-W. Chou, S.-K. Wu, M.A. Thomas, and Y.-C. Peng, J. Electron. Mater. 38 (2009) 1182-1188.

[185] S.H.L. Hongkwan Park, Felix Sunjoo Kim, Hyang Hee Choi, In Woo Cheong and Jung Hyun Kim, J. Mater. Chem. A 2 (2014) 6532-6539.

[186] O. Bubnova, Z.U. Khan, A. Malti, S. Braun, M. Fahlman, M. Berggren, and X. Crispin, Nat. Mater. 10 (2011) 429-433.

[187] L. Stepien, A. Roch, S. Schlaier, I. Dani, A. Kiriy, F. Simon, M.v. Lukowicz, and C. Leyens, Energ. Harvesting Syst. 3 (2016) 101-111.

[188] Z. Fan, D. Du, Z. Yu, P. Li, Y. Xia, and J. Ouyang, ACS Appl. Mater. Interfaces 8 (2016) 23204-23211.

[189] J. Luo, D. Billep, T. Waechtler, T. Otto, M. Toader, O. Gordan, E. Sheremet, J. Martin, M. Hietschold, and D.R. Zahn, J. Mater. Chem. A 1 (2013) 7576-7583.

[190] Z. Fan, D. Du, H. Yao, and J. Ouyang, ACS Appl. Mater. Interfaces 9 (2017) 11732-11738.

[191] S.-K. Kim, J.-H. Mo, J.-Y. Kim, and K.-S. Jang, e-Polymers 17 (2017) 501-506.

[192] N. Kim, S. Kee, S.H. Lee, B.H. Lee, Y.H. Kahng, Y.R. Jo, B.J. Kim, and K. Lee, Adv. Mater. 26 (2014) 2268-2272.

[193] Z. Fan, P. Li, D. Du, and J. Ouyang, Adv. Energy Mater. 7 (2017) 1602116.

[194] S.-M. Kim, C.-H. Kim, Y. Kim, N. Kim, W.-J. Lee, E.-H. Lee, D. Kim, S. Park, K. Lee, J. Rivnay, and M.-H. Yoon, Nat. Commun. 9 (2018) 3858.

[195] B. Cho, K.S. Park, J. Baek, H.S. Oh, Y.E. Koo Lee, and M.M. Sung, Nano Lett. 14 (2014) 3321-3327.

[196] J. Tsukamoto, A. Takahashi, and K. Kawasaki, Jpn. J. Appl. Phys. 29 (1990) 125-130.

[197] A. Yadav, K.P. Pipe, and M. Shtein, J. Power Sources 175 (2008) 909-913.

[198] M.K. Kim, M.S. Kim, S.E. Jo, H.L. Kim, S.M. Lee, and Y.J. Kim. Wearable Thermoelectric Generator for Human Clothing Applications. in 2013 Transducers & Eurosensors XXVII: The 17th International Conference on Solid-State Sensors, Actuators and Microsystems (TRANSDUCERS & EUROSENSORS XXVII). 2013.

[199] M.-K. Kim, M.-S. Kim, S. Lee, C. Kim, and Y.-J. Kim, Smart Mater. Struct. 23 (2014) 105002.

[200] S.W. Finefrock, X. Zhu, Y. Sun, and Y. Wu, Nanoscale 7 (2015) 5598-5602.

[201] Z. Lu, H. Zhang, C. Mao, and C.M. Li, Appl. Energ. 164 (2016) 57-63.

[202] J. Choi, Y. Jung, S.J. Yang, J.Y. Oh, J. Oh, K. Jo, J.G. Son, S.E. Moon, C.R. Park, and H. Kim, ACS Nano 11 (2017) 7608-7614.

[203] S. Qu, Y. Chen, W. Shi, M. Wang, Q. Yao, and L. Chen, Thin Solid Films 667 (2018) 59-63.

[204] Y. Jia, L. Shen, J. Liu, W. Zhou, Y. Du, J. Xu, C. Liu, G. Zhang, Z. Zhang, and F. Jiang, J. Mater. Chem. C 7 (2019) 3496-3502.

[205] Y. Park, K. Cho, and S. Kim, Mater. Res. Bull. 96 (2017) 246-249.

[206] Y. Kim, A. Lund, H. Noh, A.I. Hofmann, M. Craighero, S. Darabi, S. Zokaei, J.I. Park, M.H. Yoon, and C. Müller, Macromol. Mater. Eng. 305 (2020) 1900749.

[207] K. Dong, X. Peng, and Z.L. Wang, Adv. Mater. 32 (2020) 1902549.

[208] Y. Du, K.F. Cai, S.Z. Shen, R. Donelsonand, J.Y. Xu, H.X. Wang, and T. Lin, RSC Adv. 7 (2017) 43737-43742.

[209] L.K. Allison and T.L. Andrew, Adv. Mater. Technol. 4 (2019) 1800615.

[210] Q. Wu and J. Hu, Smart Mater. Struct. 26 (2017) 045037.

[211] R.A. Kishore, A. Nozariasbmarz, B. Poudel, M. Sanghadasa, and S. Priya, Nat. Commun. 10 (2019) 1765.

Wen-Yi Chen received his bachelor's degree from the University of Queensland in 2018. He is a research candidate for a master's degree at the University of Queensland. His current research focuses on fiber-based thermoelectric materials and devices under the supervision of Professor Zhi-Gang Chen and Dr Xiao-Lei Shi.

Xiao-Lei Shi is currently a Research Fellow of Energy Materials at the University of Southern Queensland. He received his Ph.D degree in 2019 from the University of Queensland under the supervision of Prof. Jin Zou and Prof. Zhi-Gang Chen with a research focus on the development of high-performance thermoelectrics and underlying physics and chemistry.

Jin Zou is currently the Chair of Nanoscience at the University of Queensland. He received his Ph.D. in Materials Physics in late 1993 from Sydney University, Australia, and worked there for 10 years with various prestigious fellowships, including an Australian Government's Queen Elizabeth II Fellowship. In the second half of 2003, Professor Zou moved to the University of Queensland and continued his research in the field of semiconductor nanostructures for energy-related applications.

Zhi-Gang Chen is currently a Professor of Energy Materials in the University of Southern Queensland (USQ). He received his Ph.D in materials science and engineering from the Institute of Metal Research, Chinese Academy of Science, in 2008. After his Ph.D., he had worked at the University of Queensland for seven years before moving to USQ, in 2016. His research concentrates on smart functional materials for thermoelectrics and nanoelectronics from synthesizing materials to understanding their underlying physics and chemistry.

Graphical Abstract

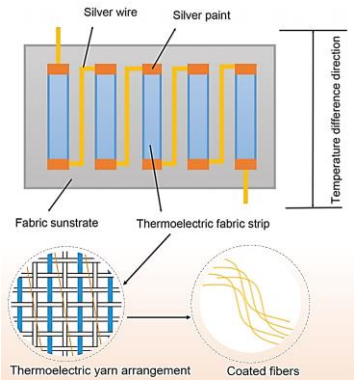

Declaration of interests

☒ The authors declare that they have no known competing financial interests or personal relationships that could have appeared to influence the work reported in this paper.

☐The authors declare the following financial interests/personal relationships which may be considered as potential competing interests:

Highlights

- A state-of-the-art review of fiber-based thermoelectrics;
- Fundamentals of performance, flexibility, and wearability are summarized;
- The progress of inorganic fibers, organic fibers, and hybrid fibers is overviewed;
- The applications of fiber-based thermoelectric devices are discussed.